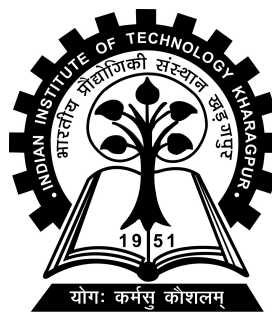


Aspects of Fractional Quantum Hall Effect in Graphene

Project-2 (PH47202) report submitted to
Indian Institute of Technology Kharagpur
in partial fulfilment for the award of the degree of
Integrated MSc
in
Physics
by
Sparsh Gupta
(21PH23005)

Under the supervision of
Professor Sudhansu Sekhar Mandal



Department of Physics
Indian Institute of Technology Kharagpur
Spring Semester, 2024-25
April 20, 2025

DECLARATION

I certify that

- (a) The work contained in this report has been done by me under the guidance of my supervisor.
- (b) The work has not been submitted to any other Institute for any degree or diploma.
- (c) I have conformed to the norms and guidelines given in the Ethical Code of Conduct of the Institute.
- (d) Whenever I have used materials (data, theoretical analysis, figures, and text) from other sources, I have given due credit to them by citing them in the text of the thesis and giving their details in the references. Further, I have taken permission from the copyright owners of the sources, whenever necessary.

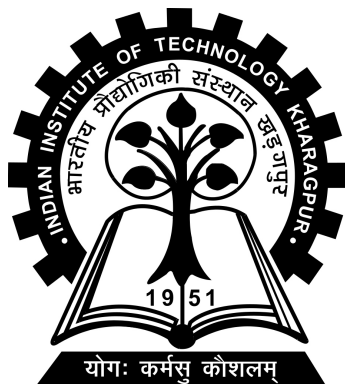
Date: April 20, 2025

Place: Kharagpur

(Sparsh Gupta)

(21PH23005)

DEPARTMENT OF PHYSICS
INDIAN INSTITUTE OF TECHNOLOGY KHARAGPUR
KHARAGPUR - 721302, INDIA



CERTIFICATE

This is to certify that the project report entitled "Aspects of Fractional Quantum Hall Effect in Graphene" submitted by Sparsh Gupta (Roll No. 21PH23005) to Indian Institute of Technology Kharagpur towards partial fulfilment of requirements for the award of degree of Integrated MSc in Physics is a record of bona fide work carried out by him under my supervision and guidance during Spring Semester, 2024-25.

Professor Sudhansu Sekhar Mandal

Date: April 20, 2025

Department of Physics

Place: Kharagpur

Indian Institute of Technology Kharagpur

Kharagpur - 721302, India

Abstract

Name of the student: **Sparsh Gupta**

Roll No: **21PH23005**

Degree for which submitted: **Integrated MSc**

Department: **Department of Physics**

Thesis title: **Aspects of Fractional Quantum Hall Effect in Graphene**

Thesis supervisor: **Professor Sudhansu Sekhar Mandal**

Month and year of thesis submission: **April 20, 2025**

In this thesis, I have presented a brief overview on the nature of the fractional quantum Hall effect (FQHE) in monolayer and bilayer graphene (MLG BLG). I started with describing the Landau-level spectrum of both MLG and BLG using the tight-binding approximation. Then I mentioned about the advantages that the Physics of Graphene offers over Ga-As-based materials in exploring strongly correlated states of two-dimensional electrons by tuning the effective electron interaction by the dielectric environment of the sample. The tunability of the interactions can be used to realize and stabilize various strongly correlated phases and explore the transitions between them. The distinct Landau-level spectrum of BLG is predicted to support a nonabelian even-denominator FQH state similar to the 5/2 state first identified in GaAs. However, the nature of this state has remained difficult to characterize. The sensitivity of the even-denominator states to both filling fraction and transverse displacement field provides new opportunities for tunability. BLG is a platform in which topological ground states with possible nonabelian excitations can be manipulated and controlled. For certain values of Electric and Magnetic fields,

we observe 4 even denominator FQH states and I have attempted to calculate how energy eigenvalues varies with Electric and Magnetic field, to observe landau level crossings at different electric and magnetic fields and its interpretation and how does this explains the formation of even denominator states. This work contributes towards a deeper theoretical understanding of the fractional quantum Hall effect in graphene and highlights the key physical mechanisms that stabilize novel correlated phases in systems with tunable band structures and interactions.

Acknowledgements

I would like to express my deepest gratitude to my supervisor, Prof. Sudhansu Sekhar Mandal, for his insightful guidance, and continuous encouragement throughout the course of this thesis. I am also immensely grateful to Tania Patra Mam (Research Scholar), whose mentorship and day-to-day discussions helped me navigate this project. This work would not have been possible without their consistent support, and I consider myself extremely fortunate to have had the opportunity to learn under their supervision. Lastly, I am grateful to my friends and family for providing an emotionally supportive environment during this academic journey.

Contents

Declaration	i
Certificate	ii
Abstract	iii
Acknowledgements	v
Contents	vi
1 Landau Levels in Monolayer Graphene	1
1.1 Introduction	1
1.2 Energy dispersion	2
1.3 Expansion around Fermi Energy	5
1.4 Landau levels	7
2 Landau Levels in Bilayer Graphene	10
2.1 Introduction	10
2.2 Electronic Structure	11
2.3 Landau Levels	12
3 Pseudopotential description of Interacting electrons	15
3.1 Pseudopotentials for conventional semiconductor systems	15
3.2 Pseudopotentials in MLG	18
4 Tunable Electron Interactions and Fractional Quantum Hall States in Graphene	20
4.1 The Challenges with Ga-As based samples	20
4.2 Model	21
4.3 Conclusion from the experiment	23
5 Even-denominator fractional quantum Hall states in Bilayer Graphene	24
5.1 Non-Abelian state in GaAs	24
5.2 Non Abelian states in BLG	25

5.3	Gapped Bilayer Graphene	29
6	Energy Gaps between even denominator states	31
6.1	Constructing the Hamiltonian	31
6.2	Landau Level diagrams	32
6.3	Conclusion	56
 Bibliography		 58

Chapter 1

Landau Levels in Monolayer Graphene

1.1 Introduction

Graphene is a 2D monoatomic crystal which, although it is proven to be thermodynamically unstable, but it becomes intrinsically stable by gentle crumpling in third dimension. This leads to a gain in elastic energy but suppress thermal vibrations which above a certain temperature can minimize the total free energy. Because of its unusual electronic energy dispersion, graphene has led to the emergence of concept of 'relativistic' particles in condensed-matter. In condensed matter physics, the Schrödinger equation is quite sufficient to describe electronic properties of materials. Graphene is an exception - its charge carriers mimic relativistic particles and are more easily and naturally described starting with the Dirac equation rather than the Schrödinger. The relativistic behavior of electron in graphene brought about new possibilities for testing relativistic phenomena, some of which are unobservable in high-energy physics. Among the most spectacular phenomena reported so far are

the new quantum Hall effects.

One of the effects that change their form - comparing to the electrons described by Schrödinger equation - are also Landau levels. These are quantized energy levels for electrons in a magnetic field. They still appear also for relativistic electrons, just their dependence on field and quantization parameter is different.

1.2 Energy dispersion

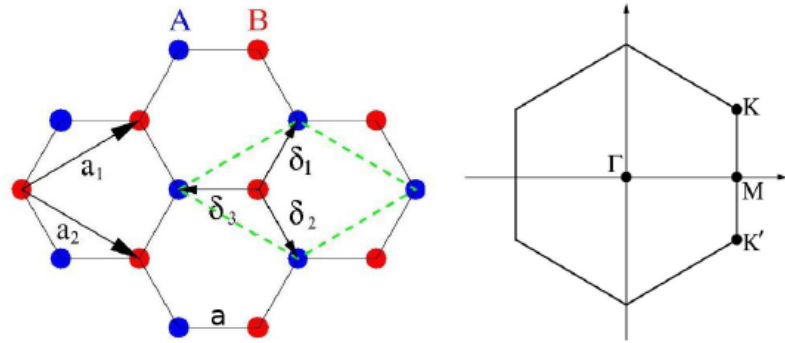


FIGURE 1.1: left:Bravais lattice with primitive vectors a_1 ; a_2 ($a = 0.142\text{nm}$) and marked sublattices A and B, right: first Brillouin zone with marked corners K,K' of different symmetry

As shown in figure 1.1 let us name the primitive vectors in real space as a_1 and a_2 and in reciprocal lattice as b_1 and b_2 . The real space lattice vectors and the corresponding reciprocal ones are:

$$\vec{a}_{1,2} = \frac{\sqrt{3}a}{2}(\sqrt{3}, \pm 1), \quad \vec{b}_{1,2} = \frac{2\pi}{\sqrt{3}a}(1/\sqrt{3}, \pm 1)$$

The first Brillouin zone is a hexagon, where the corners form two inequivalent groups of K points, traditionally labelled K and K' with:

$$\mathbf{K} = \frac{2\pi}{3a}(1, \frac{1}{\sqrt{3}}), \quad \mathbf{K}' = \frac{2\pi}{3a}(1, -\frac{1}{\sqrt{3}})$$

We start from the tight-binding model for the carbon π band. In the tight-binding model, the wavefunction is given by:

$$\Psi(r) = \sum_{\mathbf{R}_A} \psi_A(\mathbf{R}_A) \phi(r - \mathbf{R}_A) + \sum_{\mathbf{R}_B} \psi_B(\mathbf{R}_B) \phi(r - \mathbf{R}_B)$$

where $\phi(r)$ is the wavefunction of p_z orbital of Carbon atom which composes π band, $\mathbf{R}_A = n_a \mathbf{a} + n_b \mathbf{b} + \tau_1$ and $\mathbf{R}_B = n_a \mathbf{a} + n_b \mathbf{b}$ with n_a, n_b being integers. Let $-\gamma_0$ be the transfer integral between nearest neighbour carbon atom.

$\Psi(r)$ represents the wavefunction of electron in Graphene. The electron could be at site A or site B, so $\Psi(r)$ is in superposition state of electron wavefunction at site A, $|\psi_A\rangle$ and at site B, $|\psi_B\rangle$. $|\psi_A\rangle$, which is the electron wavefunction at site A will be in superposition of all the wavefunctions at different \mathbf{R}_A positions, so $|\psi_A\rangle$ can be written as (inserting identity operator):

$$|\psi_A\rangle = \sum_{R_A} |R_A\rangle \langle R_A| \psi_A \rangle$$

$\langle R_A| \psi_A \rangle$ is nothing but $\psi_A(R_A)$ which is the Bloch function that can be written as $e^{ik \cdot R_A} f_A(k)$. The same comments can be made for $|\psi_B\rangle$.

The Hamiltonian is then given by:

$$H = -\gamma_0 \sum_{\mathbf{R}_A} \sum_{l=1}^3 \left[|R_A\rangle \langle R_A - \tau_l| + |R_A + \tau_l\rangle \langle R_A| \right]$$

where $|R\rangle$ represents $\phi(r - R)$, i.e., the atomic state localised at site R. The Schrodinger Equation then becomes:

$$\epsilon \psi_A(R_A) = -\gamma_0 \sum_{\mathbf{R}_A} \sum_{l=1}^3 |R_A - \tau_l\rangle e^{ik \cdot R_A} f_A(k)$$

$$\epsilon \psi_B(R_B) = -\gamma_0 \sum_{\mathbf{R}_B} \sum_{l=1}^3 |R_B + \tau_l\rangle e^{ik \cdot R_B} f_B(k)$$

The Hamiltonian matrix can then be calculated.

$$\begin{aligned}
 & \langle \psi_A | H | \psi_A \rangle = \langle \psi_B | H | \psi_B \rangle = 0 \\
 & \langle \psi_B | H | \psi_A \rangle = -\gamma_0 \sum_{l=1}^3 e^{ik\tau_l} f_B^*(k) f_A(k), \quad \langle \psi_A | H | \psi_B \rangle = -\gamma_0 \sum_{l=1}^3 e^{-ik\tau_l} f_A^*(k) f_B(k) \\
 H_{AB} &= \langle \psi_A | H | \psi_B \rangle \\
 &= \begin{bmatrix} f_A^*(k) & f_B^*(k) \end{bmatrix} \begin{bmatrix} 0 & h(k) \\ h^*(k) & 0 \end{bmatrix} \begin{bmatrix} f_A(k) \\ f_B(k) \end{bmatrix}
 \end{aligned}$$

where $h(k) = -\gamma_0 \sum_{l=1}^3 e^{ik\tau_l}$. Now $H\psi = \epsilon\psi$.

$$\epsilon^2 = |h(k)|^2$$

From figure 1.1, we can determine δ_l .

$$\vec{\delta}_1 = \frac{a}{2}(1, \sqrt{3})$$

$$\vec{\delta}_2 = \frac{a}{2}(1, -\sqrt{3})$$

$$\vec{\delta}_3 = a(-1, 0)$$

Using above δ_l and on further simplification, we obtain:

$$\epsilon_{\pm} = \pm \gamma_0 \sqrt{1 + 4 \cos\left(\frac{3k_x a}{2}\right) \cos\left(\frac{\sqrt{3}k_y a}{2}\right) + 4 \cos^2\left(\frac{\sqrt{3}k_y a}{2}\right)}$$

Here ϵ_+ and ϵ_- give the eigenenergies for the conduction and valence bands, respectively. These two bands touch each other at the K and K' points (also known as the Dirac points) where $\epsilon_{\pm} = 0$. They are shown in figure 1.2 .

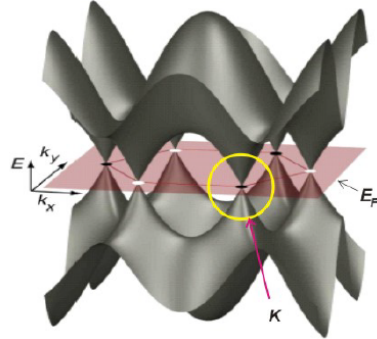


FIGURE 1.2: Energy dispersion with two band for the p_z electrons; red plane indicates the Fermi level

1.3 Expansion around Fermi Energy

In the vicinity of K point (or K' point), we write k as $K + k$ with $|k| \ll 1$, we calculate the ϵ at $K + k$ and on further simplification, we obtain linear energy dispersion relation:

$$\epsilon_K = \pm \hbar v_F |k|$$

where $v_F = \frac{3a\gamma_0}{2\hbar}$. We get the same dispersion relation at K' point. The are shown in figure 1.3 .

We know that energy dispersion which is linear in wave vector belongs to massless

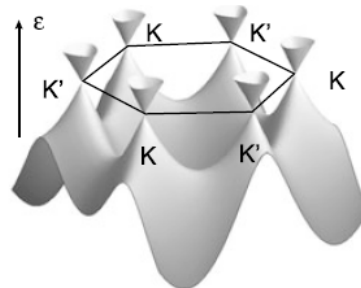


FIGURE 1.3: π band structure of Graphene in the nearest neighbour tight binding model

particles. We say that electrons and holes with wave vectors close to K and K'

points behave as massless. These massless particles are described by Dirac equation and not Schrodinger equation. Since particles behave as massless only around the K and K', we can expand the Hamiltonian in vicinity of Dirac points and on further calculations and simplifications, we obtain the following Hamiltonian matrix:

$$H(q) = \hbar v_F \begin{bmatrix} 0 & i(k_x - ik_y)e^{\frac{-i\pi}{3}} \\ -i(k_x + ik_y)e^{\frac{i\pi}{3}} & 0 \end{bmatrix}$$

We can redefine the wavefunctions as:

$$\Psi_0^K = \begin{bmatrix} f_A(k) \\ f_B(k) \end{bmatrix} \implies \Psi^K = \begin{bmatrix} ie^{\frac{-i\pi}{3}} f_A(k) \\ f_B(k) \end{bmatrix}$$

We can then redefine the Hamiltonian matrix in vicinity of K point considering the redefined wavefunction as:

$$H(q) = \hbar v_F \begin{bmatrix} 0 & i(k_x - ik_y) \\ -i(k_x + ik_y) & 0 \end{bmatrix} = \hbar v_F \left(\begin{bmatrix} 0 & k_x \\ k_x & 0 \end{bmatrix} + \begin{bmatrix} 0 & -ik_y \\ ik_y & 0 \end{bmatrix} \right)$$

$$H_K(q) = \hbar v_F \vec{\sigma} \cdot \vec{k}$$

Similarly, we can calculate Hamiltonian matrix at K' point. We will find that $H_{K'}(q) = -H_K^T(q)$. In relation with Dirac equation, we call the wavefunction Ψ^β spinor. In its upper and lower term it has the quantum mechanical amplitudes of finding the particle in one of the two sublattices A and B, respectively. And for each valley K and K' we have one such spinor. If we put them together in one bispinor $\Psi = (\Psi^{K'}, \Psi^K)$ and both Hamiltonian in a common one, we get

$$H = v_F \begin{bmatrix} -\vec{\sigma}^* \cdot \vec{k} & 0 \\ 0 & \vec{\sigma} \cdot \vec{k} \end{bmatrix}$$

1.4 Landau levels

In a conventional electron gas (non-relativistic) Landau quantization produces equidistant energy levels, which is due to the parabolic dispersion law of free electrons. In graphene the electrons have relativistic dispersion law, which strongly modifies the Landau quantization of the energy and the position of the levels. We make the substitution, $p_i \implies p_{0i} = p_i - \frac{e}{c}A_i$. The Hamiltonian will change to

$$H = v_F \begin{bmatrix} 0 & -(p_{0x} + ip_{0y}) & 0 & 0 \\ -(p_{0x} - ip_{0y}) & 0 & 0 & 0 \\ 0 & 0 & 0 & (p_{0x} - ip_{0y}) \\ 0 & 0 & (p_{0x} + ip_{0y}) & 0 \end{bmatrix}$$

where the 4 component wavefunction corresponds to $\Psi = \begin{bmatrix} \Phi_A^{K'} \\ \Phi_B^{K'} \\ \Phi_A^K \\ \Phi_B^K \end{bmatrix}$

Because equations for K and K' valley are decoupled, let us first look for the solutions of the K valley. We are solving the system

$$\epsilon\Phi_A^K = v_F(\hat{p}_{0x} - i\hat{p}_{0y})\Phi_B^K$$

$$\epsilon\Phi_B^K = v_F(\hat{p}_{0x} + i\hat{p}_{0y})\Phi_A^K$$

which can be by inserting one equation into another further decoupled into

$$\epsilon^2\Phi_A^K = v_F^2(\hat{p}_{0x} - i\hat{p}_{0y})(\hat{p}_{0x} + i\hat{p}_{0y})\Phi_A^K$$

$$\epsilon^2\Phi_B^K = v_F^2(\hat{p}_{0x} + i\hat{p}_{0y})(\hat{p}_{0x} - i\hat{p}_{0y})\Phi_B^K$$

For the magnetic field orthogonal to the graphene layer, the vector potential can be chosen in Landau gauge as $A = (-By; 0)$. For such gauge, $[H, \hat{p}_x] = 0$. Using this and on performing the calculations for Φ_B^K , we can get the energy values for Landau

levels in graphene monolayer satisfying

$$\frac{\epsilon^2}{v_F^2} = \frac{he_0B}{c}(2n + 1 - 1)$$

where $n = 0, 1, 2, \dots$ goes through the same values as for harmonic oscillator. Since ϵ has positive and negative roots, we can extend the domain of n to integer values and write energy levels as

$$\epsilon = sgn(n) \sqrt{\frac{2he_0B}{c}} v_F \sqrt{|n|} = \hbar\omega^{Dirac} sgn(n) \sqrt{|n|}$$

where, $\omega^{Dirac} = v_F \sqrt{\frac{2e_0B}{\hbar c}}$. The Landau level index, n , can be positive or negative. The positive values correspond to electrons (conduction band), while the negative values correspond to holes (valence band). Furthermore, they are not equidistant as in conventional case and the largest energy separation is between the zero and the first Landau level. This large gap allows one to observe the quantum Hall effect in graphene, even at room temperature.

If we do similar calculations for Φ_A^K , we get

$$\frac{\epsilon^2}{v_F^2} = \frac{he_0B}{c} 2(n + 1)$$

with $n = 0, 1, \dots$. In terms of the occupation of the sublattices A and B, we can therefore expect interesting properties. The wavefunction at LL $n \neq 0$ should always have non-zero amplitudes on both sublattices A and B, while the wavefunctions at the Landau level $n = 0$ should have non-zero amplitude only on one sublattice: B sublattice for valley K or A sublattice for valley K'. This property of the wavefunctions for the LLs in graphene makes the $n = 0$ level very special for different magnetic applications of graphene.

The wavefunctions are given by following expressions.

$$\Psi_{n,k}^K = \frac{C_n}{\sqrt{L}} e^{-ikx} \begin{bmatrix} 0 \\ 0 \\ sgn(n)(-i)\phi_{|n|-1,k} \\ \phi_{|n|,k} \end{bmatrix}$$

$$\Psi_{n,k}^{K'} = \frac{C_n}{\sqrt{L}} e^{-ikx} \begin{bmatrix} \phi_{|n|,k} \\ sgn(n)(-i)\phi_{|n|-1,k} \\ 0 \\ 0 \end{bmatrix}$$

Here L^2 is area of the system. $C_n = 1$ for $n = 0$ and $C_n = \frac{1}{\sqrt{2}}$ for $n \neq 0$.

$$\phi_{|n|,k} \propto \exp\left(\frac{-1}{2} \frac{(y - kl_B^2)^2}{l_B^2}\right) H_n\left[\frac{(y - kl_B^2)}{l_B}\right]$$

$\phi_{|n|,k}$ is the wavefunction for non-relativistic electron at nth LL. We observe that the wavefunction at both sites A and B will be different for valley K and K' which must differ in their index n for 1 to yield the same energy eigenvalue for both.

Chapter 2

Landau Levels in Bilayer Graphene

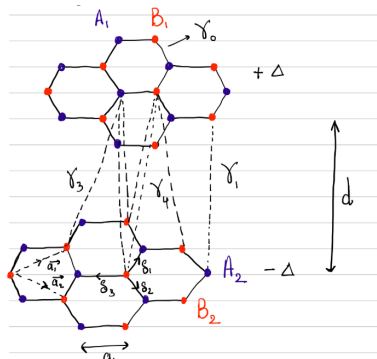


FIGURE 2.1: The lattice structure of AB-stacked bilayer graphene

2.1 Introduction

The most stable structure of bilayer graphene is known to be AB (Bernal) stacking as shown in figure 2.1. A unit cell includes A_1 and B_1 atoms on layer 1 and A_2 and B_2 on layer 2, and the layers are stacked with the interlayer spacing of $d \approx 0.334$ nm, such that pairs of sites B_1 and A_2 lie directly above or below each other. The

interlayer coupling drastically changes the linear band structure of monolayer, leaving a pair of quadratic energy bands touching at zero energy.

The parameter γ_0 describes nearest-neighbor coupling between A_i and B_i within each layer. γ_1 describes the strong nearest layer couplings between sites $B_1 - A_2$ that lie directly above or below each other. γ_3 describes nearest-layer coupling between sites $A_1 - B_2$ and γ_4 is another nearest layer coupling between $A_1 - A_2$ and between $B_1 - B_2$.

2.2 Electronic Structure

We can again write the Hamiltonian for Bilayer Graphene using tight binding approximation. We get the following:

$$\begin{aligned} H = & \left(-\gamma_0 \sum_{R_{A_1}, R_{A_2}} \sum_{l=1}^3 |R_{A_1}\rangle \langle R_{A_1} - \delta_l| + |R_{A_1} - \delta_l\rangle \langle R_{A_1}| + \right. \\ & |R_{A_2}\rangle \langle R_{A_2} - \delta_l| + |R_{A_2} - \delta_l\rangle \langle R_{A_2}| \Big) \\ & + \left(-\gamma_1 \sum_{R_{B_1}, R_{A_2}} |R_{B_1}\rangle \langle R_{A_2}| + |R_{A_2}\rangle \langle R_{B_1}| \right) \\ & + \left(-\gamma_3 \sum_{R_{A_1}, R_{A_2}} \sum_{l=1}^3 |R_{A_1}\rangle \langle R_{A_2} - \delta_l| + |R_{A_2} - \delta_l\rangle \langle R_{A_1}| \right) \\ & + \left. \left(-\gamma_4 \sum_{R_{A_1}, R_{A_2}, R_{B_1}, R_{B_2}} \sum_{l=1}^3 |R_{A_1}\rangle \langle R_{B_2} + \delta_l| + |R_{B_2} + \delta_l\rangle \langle R_{A_1}| + \right. \right. \\ & |R_{B_1}\rangle \langle R_{A_2} - \delta_l| + |R_{A_2} - \delta_l\rangle \langle R_{B_1}| \Big) \end{aligned}$$

We consider the basis as $(|A_1\rangle, |B_1\rangle, |A_2\rangle, |B_2\rangle)$. Similar to what we did for monolayer graphene, we can determine the Hamiltonian matrix in general and then exclusively calculate near either of the Dirac points K or K'. The calculation is long and complicated, but we obtain the following result of the Hamiltonian matrix at K:

$$H_K = \begin{bmatrix} 0 & \nu p_- & -\nu_4 p_- & \nu_3 p_+ \\ \nu p_+ & 0 & -\gamma_1 & -\nu_4 p_- \\ -\nu_4 p_+ & -\gamma_1 & 0 & \nu p_- \\ \nu_3 p_- & -\nu_4 p_+ & \nu p_+ & 0 \end{bmatrix}$$

where $\nu = \frac{\sqrt{3}a\gamma_0}{2\hbar}$, $\nu_3 = \frac{\sqrt{3}a\gamma_3}{2\hbar}$, $\nu_4 = \frac{\sqrt{3}a\gamma_4}{2\hbar}$ and $p_{\pm} = (p_x \pm ip_y)$. The effective Hamiltonian for K' can be obtained by exchanging p_+ and p , giving the equivalent spectrum in zero magnetic field. We neglect the parameters ν_3 and ν_4 as they give minor effects to band structure. Then the eigenenergies of above Hamiltonian becomes:

$$\epsilon_{\mu,s}(p) = s \left[\frac{\mu}{2} \gamma_1 + \sqrt{\frac{1}{2} \gamma_1^2 + \nu^2 p^2} \right]$$

The energy bands can be seen in figure 2.2 where Δ is the interlayer potential asymmetry. The branch $\mu = -$ gives a pair of conduction ($s = +$) and valence ($s = -$) bands touching at zero energy. The other branch $\mu = +$ is another pair repelled away by $\pm\gamma_1$. In the following we use the notation $\mu = H, L$ instead of $+, -$ and specify the four energy bands as $(\mu, s) = (L, \pm), (H, \pm)$. We will also use the notation the band indexes 1, 2, 3, 4 for $(H, -), (L, -), (L, +), (H, +)$, respectively, in the ascending order in energy. In $\epsilon \ll \gamma_1$, the lower subbands $(L, -)$ and $(L, +)$ are approximately expressed as a quadratic form,

$$\epsilon_{L,\pm} \approx \pm \frac{\nu^2 p^2}{\gamma_1} \equiv \frac{p^2}{2m^*}$$

with the effective mass $m^* = \frac{\gamma_1}{2\nu^2}$.

2.3 Landau Levels

Similar to what we did for Monolayer graphene, we substitute p_i with $\pi_i = p_i + \frac{e}{c}A_i$. The Landau level spectrum can be found using the relation $\pi_+ = \left(\frac{\sqrt{2}\hbar}{l_B}\right)a^\dagger$ and

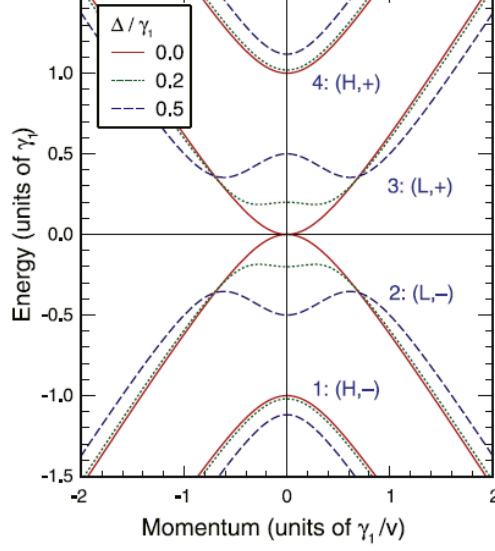


FIGURE 2.2: energy dispersion of bilayer graphene with various values of inter-layer potential asymmetry Δ

$\pi_- = \left(\frac{\sqrt{2}\hbar}{l_B} \right) a$. Here $l_B = \sqrt{\frac{e\hbar}{eB}}$ and a^\dagger and a are raising and lowering operators, respectively, which operate on the Landau-level wavefunction ϕ_n as $a\phi_n = \sqrt{n}\phi_{n-1}$ and $a^\dagger\phi_n = \sqrt{n+1}\phi_{n+1}$. The eigenfunction can be written as $(c_1\phi_{n-1}, c_2\phi_n, c_3\phi_n, c_4\phi_{n+1})$. For $n \geq 1$, the Hamiltonian matrix for vector (c_1, c_2, c_3, c_4) then becomes at K point,

$$H = \begin{bmatrix} 0 & \hbar\omega_B\sqrt{n} & 0 & 0 \\ \hbar\omega_B\sqrt{n} & 0 & -\gamma_1 & 0 \\ 0 & -\gamma_1 & 0 & \hbar\omega_B\sqrt{n+1} \\ 0 & 0 & \hbar\omega_B\sqrt{n+1} & 0 \end{bmatrix}$$

where $\hbar\omega_B = \frac{\sqrt{2}\hbar\nu}{l_B}$. We can get the 4 eigenvalues:

$$\epsilon_{\mu,s,n} = \frac{s}{\sqrt{2}} \left[\gamma_1^2 + (2n+1)(\hbar\omega_B)^2 + \mu \sqrt{\gamma_1^4 + 2(2n+1)\gamma_1^2(\hbar\omega_B)^2 + (\hbar\omega_B)^4} \right]^{\frac{1}{2}}$$

For $n = 0$, the first component of the wave function disappears and we have three levels,

$$\epsilon_{L,0} = 0$$

,

$$\epsilon_{H,s,0} = s\sqrt{\gamma_1^2 + (\hbar\omega_B)^2}$$

For $n = -1$, only the last component survive, leaving a single level:

$$\epsilon_{L,-1} = 0$$

Each Landau level is degenerate in valley and spin. The zero-energy level is 8-fold degenerate due to the extra degeneracy of $\epsilon_{L,0} = \epsilon_{L,-1}$, while all others are fourfold degenerate as in monolayer graphene. In low energy region, $\epsilon \ll \gamma_1$, the Landau levels of the lower subband L approximate:

$$\epsilon_{L,s,n} \approx s \frac{\hbar e B}{m^*} \sqrt{n(n+1)} (n = 0, 1, 2, \dots)$$

Chapter 3

Pseudopotential description of Interacting electrons

3.1 Pseudopotentials for conventional semiconductor systems

In the context of the FQHE, Haldane pseudopotentials provide a powerful way to describe the interaction between two electrons confined to a single Landau level. The magnetic field is so strong that the spacing between the Landau levels are (in the absence of any disorder) much larger than any other form of energy. In that situation, the Hamiltonian of the system is simply the projected interparticle interaction. Haldane pointed out that the interaction energy of a pair of particles with the same Landau indices can be written as

$$H_{ij} = \sum_{m=0}^{\infty} V_m P_{ij}^m$$

where P_{ij}^m projects the pair of particles i, j onto the relative angular momentum m. Antisymmetry of the electron wave function indicates that m is an odd integer. The parameters V_m are the so-called Haldane pseudopotentials, which are defined as the energy of two electrons with the relative angular momentum m. They are determined by the structure of the wave functions of the corresponding Landau level and for the n-th Landau level can be found from the following expression

$$V_m^{(n)} = \int_0^\infty \frac{dq}{2\pi} q V(q) [F_n(q)]^2 L_m(q^2) e^{-q^2}$$

where $L_m(x)$ are the Laguerre polynomials, $V(q) = \frac{2\pi e^2}{\kappa q l_0}$ is the Coulomb interaction in momentum space, κ is the background dielectric constant, and $F_n(q)$ is the form factor of the nth Landau level. The form factor is completely determined by the nth Landau level wave functions. For conventional semiconductor systems, the form factors have the following form

$$F_n(q) = L_n(q^2/2)$$

Therefore, any translationally and rotationally invariant two-body interaction, projected to a single Landau level can be described completely by a set of pseudopotentials.

The Haldene pseudopotentials at LLL can also be written as:

$$V_m = \frac{\langle M, m | V | M, m \rangle}{\langle M, m | M, m \rangle}$$

where

$$|M, m\rangle \approx (z_1 + z_2)^M (z_1 - z_2)^m e^{\frac{-(|z_1|^2 + |z_2|^2)}{4l_B^2}}$$

is the 2 particle wavefunction at the LLL with M describing angular momentum of the centre of mass and m describing relative angular momentum. For central potentials, they do not depend on the overall angular momentum M. These eigenvalues

capture a crude picture of the spatial profile of the potential. This is because, as we have seen, the wavefunctions $|M, m\rangle$ are peaked on a circle of radius $r \approx \sqrt{2m}l_B$. Correspondingly, the eigenvalues are roughly

$$V_m \approx V(r = \sqrt{2m}l_B)$$

This means that typically the V_m are positive for a repulsive potential and negative for an attractive potential, in each case falling off as $V(r)$ as m increases.

Importantly, however, the eigenvalues are discrete. It means that each of the states $|M, m\rangle$ can be thought of as a bound state of two particles, even if the potential is repulsive! This is in stark contrast to quantum mechanics in the absence of a magnetic field where there are no discrete-energy bound states for a repulsive potential, only scattering states with a continuous spectrum. But the magnetic field changes this behaviour.

We can also calculate pseudopotentials at higher LLs:

$$V_m^{(n)} = \frac{1}{(n!)^2} \frac{\langle M, m | a_i^n a_j^n V(|r_i - r_j|) a_i^{\dagger n} a_j^{\dagger n} | M, m \rangle}{\langle M, m | M, m \rangle}$$

We can think of particles in the n th Landau level, interacting through a potential V as equivalent to particles in the lowest Landau level interacting with potential $V_m^{(n)}$. Typically one finds that the values of $V_m^{(n)}$ are smaller than the values of V_m for low m . This means that there's less of a penalty paid for particles coming close at higher LLs.

3.2 Pseudopotentials in MLG

For the n -th graphene Landau level, the Form factors are given by the following expressions

$$F_0(q) = L_0(q^2/2)$$

$$F_n(q) = \frac{1}{2} \left[L_n\left(\frac{q^2}{2}\right) + L_{n-1}\left(\frac{q^2}{2}\right) \right]$$

With these form factors the pseudopotentials for graphene are then calculated. The pseudopotentials are given in units of the Coulomb energy, $\epsilon_C = \frac{e^2}{\kappa l_0}$, where κ is the background dielectric constant of the system.

To compare the interaction properties of graphene and the conventional nonrelativistic systems, we present in figure 3.1, the pseudopotentials calculated for graphene and for the non-relativistic system. Since the FQHE can be realized only in the low-index LLs, the results are shown only for small values of n ($n \leq 2$). For $n = 0$ graphene and a nonrelativistic system have the same pseudopotentials. In a higher LL index there is an important difference in the behavior of the pseudopotentials in these two systems.

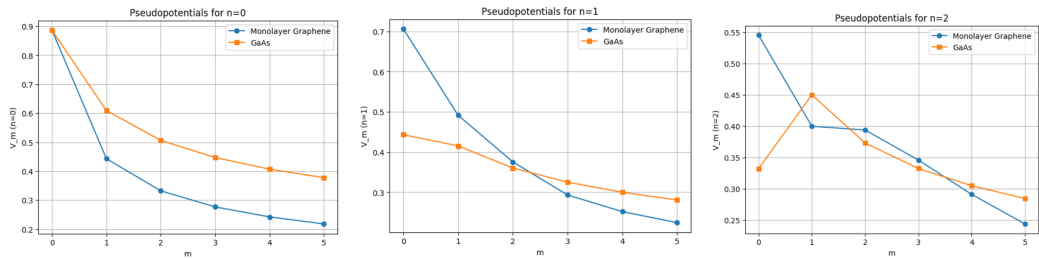


FIGURE 3.1: The Haldane pseudopotentials shown as a function of the relative angular momentum for non-relativistic and graphene systems

More specifically, for $n = 1$, the graphene system shows a stronger electron-electron repulsion, i.e., a larger pseudopotential, at small relative angular momentum,

$m < 2$, and a weaker repulsion at a large angular momentum, $m \geq 2$, compared to that for a non-relativistic system. Based on the general properties of the Laughlin incompressible state, we can conclude that the stronger repulsion at small values of the angular momentum implies a more stable FQHE state.

Due to the antisymmetry of the electronic wave functions, only the pseudopotentials with odd relative angular momenta contribute to the spin-polarized FQHE states. Hence only the pseudopotentials with $m = 1, 3, 5, \dots$ determine the spin polarized, and in the case of graphene, the valley-polarized properties of the system. For these values of m the pseudopotentials in the $n = 1$ LL show an interesting behavior: while for $m = 3$ and 5 the pseudopotential, $V_m^{(n)}$, monotonically increases with n , and for $m = 1$, the pseudopotential $V_1^{(n)}$ has a maximum at $n = 1$. Therefore the electrons with relative angular momentum $m = 1$ show the strongest repulsion in the $n = 1$ LL. This is different from the behavior of a non-relativistic system, where the strongest repulsion is in the lowest $n = 0$ LL.

The stability of the incompressible FQHE state, i.e., the magnitude of the FQHE gap, depends on how fast the pseudopotentials decay with increasing relative angular momentum. For spin and valley polarized electron systems this decay is determined by the ratios $\frac{V_1^{(n)}}{V_3^{(n)}}$ and $\frac{V_3^{(n)}}{V_5^{(n)}}$. The larger the ratios, the more stable is the FQHE.

Chapter 4

Tunable Electron Interactions and Fractional Quantum Hall States in Graphene

4.1 The Challenges with Ga-As based samples

Two-dimensional electron systems (2DES) placed in a high magnetic field exhibit strongly correlated phases characterized by fractionally quantized Hall conductivity, quasiparticles that carry a fraction of electron charge, and fractional (Abelian or possibly non-Abelian) statistics. Although many FQH states have been discovered in GaAs-based 2DES, these systems are plagued by the fact that their 2DES is buried inside a larger 3D structure. This fixes the effective interactions at values that are often not optimal for some of the most interesting FQH states, including the Read-Rezayi series. Theoretically, such states are known to be very sensitive to the form of the effective interactions.

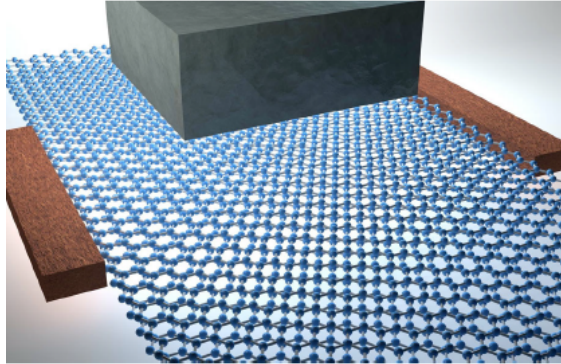


FIGURE 4.1: Setup of a graphene system with tunable electron interactions

Another problem stems from the strong dielectric screening and finite well-width in GaAs, which weakens the electron-electron interactions, thereby making FQH states fragile. This has been a major obstacle in the studies of the possibly non-Abelian states, which could only be observed in ultra-high-mobility samples. Thus, it is desirable to find an alternative high-mobility 2DES with strong effective Coulomb interactions that are adjustable in a broad range.

A promising candidate for this kind of material is MLG, where $\nu = \frac{1}{3}$ state, and several other states, has been observed before. Remarkably, due to graphene's truly 2D nature, the short range electron interactions greatly exceed those in GaAs, which leads to a significantly more robust FQH state at $\nu = \frac{1}{3}$. A closely related material, BLG has similarly high mobility, and exhibits interaction-induced quantum Hall states at integer filling factors at low magnetic fields. This indicates that, similarly to MLG, the underlying electron interactions are strong and one could expect robust FQH states in BLG as well.

4.2 Model

A graphene sample is situated in a dielectric medium with permittivity ϵ_1 , and a semi-infinite dielectric plate with permittivity $\epsilon_2 \neq \epsilon_1$ is placed at a distance $\frac{d}{2}$ away

from the graphene sheet. The setup can be seen in figure 4.1 .The effective interactions between electrons in graphene change due to the surface charges induced at the boundary between dielectrics:

$$V(r) = \frac{e^2}{\epsilon_1 r} + \alpha \frac{e^2}{\epsilon_1 \sqrt{r^2 + d^2}}, \quad \alpha = \frac{\epsilon_1 - \epsilon_2}{\epsilon_1 + \epsilon_2}$$

Below we measure the distance d in units of the magnetic length l_B and the energy in units of $e^2/\epsilon_1 l_B$. Ratio $\frac{d}{l_B}$ controls the effective interactions within a partially filled LL. The interactions can be tuned by varying the magnetic field B , which modifies the ratio $\frac{d}{l_B}$.

We project the interaction to a partially filled LL under consideration. Within a LL, $V(r)$ is parametrized by the Haldane pseudopotentials m , which can be conveniently evaluated from the Fourier transform of the Coulomb interaction, $\tilde{V}(q)$, and the form factor $F(q)$ encoding the properties of LL orbitals.

We know the relation between pseudopotential values and the stability of $\nu = \frac{1}{3}$ and $\nu = \frac{5}{2}$ states . At $\nu = \frac{1}{3}$, the bare Coulomb interaction in $n = 0$ LL favors the Laughlin state. Reducing V_1 while keeping $V_{m \geq 3}$ constant eventually destroys the gap and a compressible state sets in.

At half filling of the LLL ($\nu = \frac{1}{2}$), the Coulomb interaction gives rise to a gapless Fermi liquid of composite fermions. However, in half-filled $n = 1$ LL there is a fully developed plateau in experiments, attributed to the MR state. In numerical studies, the ground state of the Coulomb interaction at $\nu = \frac{5}{2}$ is seen to be adiabatically connected to the MR state. The overlap of the ground state with the MR state is improved by the increase in V_1 pseudopotential (or, alternatively, by reducing V_3). Therefore, theory shows that varying the first few pseudopotentials provides a convenient way to assess stability and induce transitions between FQH states. However, so far it has been difficult to find a controlled way of tuning V_m 's experimentally in a sufficiently broad range.

4.3 Conclusion from the experiment

By tuning the electron interactions in Graphene, pseudopotentials can be varied in a broad interval and FQH gaps can be enhanced several times or even reduced to zero, allowing for a more complete exploration of compressible and incompressible phases than can be attained in GaAs materials. The tunability of the interactions can be used to realize and stabilize various strongly correlated phases and explore the transitions between them. The proposed method is expected to be very efficient in optimizing the Abelian FQH states that belong to the hierarchy series.

Non-Abelian states, although expected to be stabilized, may require a more subtle approach with several dielectric plates of different permittivities and thicknesses of the order of l_B placed in the vicinity of the surface. In such a system, interactions can be tuned in a broader range and would admit a simultaneous change of several pseudopotentials that may be required for the realization of other non-Abelian and multicomponent FQH states.

Chapter 5

Even-denominator fractional quantum Hall states in Bilayer Graphene

5.1 Non-Abelian state in GaAs

The experimental observation of the even denominator fractional quantum Hall (FQH) state, appearing at $\nu = \frac{5}{2}$ filling in the $N = 1$ Landau level (LL) of GaAs, it has remained an intensely studied anomaly in condensed matter physics. Numerical calculations suggest the likely ground state to be the Moore-Read (MR) Pfaffian type of p-wave superconductor resulting from the condensation of composite Fermion pairs.

The ground state at half-filling is sensitive to the details of Coulomb interaction, and the $N = 1$ LL of GaAs proved to be optimal for stabilizing the Pfaffian state. Experimental studies indicate that the $\frac{5}{2}$ state is spin polarized, and carries $\frac{e}{4}$ fractional charge, observations which are both consistent with the Pfaffian description.

One of the most uniquely identifiable features of the Pfaffian is that its excitations are anticipated to be Majorana zero modes, obeying non-Abelian fractional statistics. However, measurement of the quantum statistics associated with the $\frac{5}{2}$ state remains an open challenge, with progress hindered by the fragile nature of the $\frac{5}{2}$ state combined with unfavorable electrostatics in GaAs.

5.2 Non Abelian states in BLG

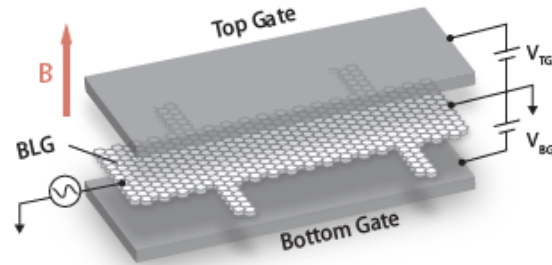


FIGURE 5.1: Schematic of the device geometry

BLG is encapsulated by hexagonal boron nitride (hBN) (figure 5.1) that offers a promising new platform for studying even denominator states. The $N = 1$ LL in BLG has an unusual composition, comprising a mixture of the conventional Landau orbital 0 and 1 wavefunctions, and moreover is accidentally degenerate with the $N = 0$ LL (figure 5.2).

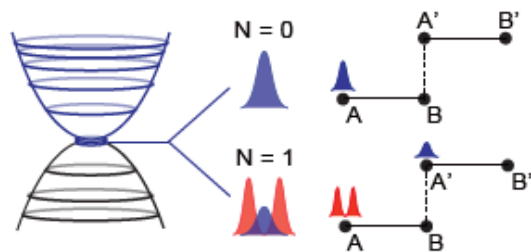


FIGURE 5.2: Energy spectrum of the BLG LLs near the charge neutrality point

Due to this construction, application of a strong magnetic field, B , can both lift the level degeneracy and modify the precise structure of the $N = 1$ wavefunction by modifying the relative weight of the conventional 0, 1 contributions. Both of these effects determine the stability of the Pfaffian ground state. Additionally, applying a transverse electric field, D , breaks the inversion symmetry between the two sets of graphene lattices, and induces phase transitions between ground states with different valley and orbital polarizations.

Application of both B and D fields therefore makes it theoretically possible to dynamically tune several key parameters within a single device, including the orbital wavefunction, effective Coulomb interaction, and Landau level mixing, all of which play critical roles in determining the nature of the even denominator state.

We utilize the dual gate geometry to tune through different orbital and layer polarizations and we observe 4 even denominator states appearing only within symmetry broken $N = 1$ orbital branches of the LLL.

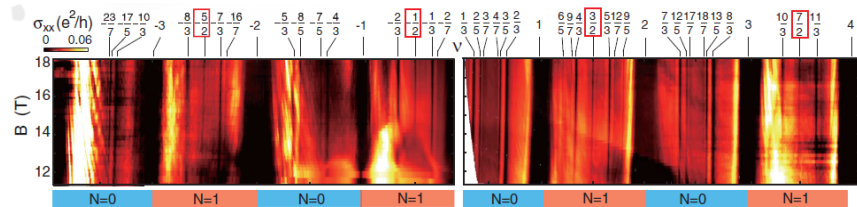


FIGURE 5.3: σ_{xx} as a function of filling factor ν and magnetic field B at (left) $D = 100$ mV/nm, (right) $D = 35$ mV/nm for the LLL ($-4 \leq \nu \leq 4$).

The high device quality is evident by the ability to resolve all of the broken-symmetry IQHE states, as well as the numerous FQH states observed throughout the phase space. Most remarkable is the appearance of conductance minima, suggestive of several even-denominator states, occurring at filling fractions $-\frac{5}{2}, -\frac{1}{2}, \frac{3}{2}$ and $\frac{7}{2}$. We observe that these states appear only at half filling of the broken-symmetry states

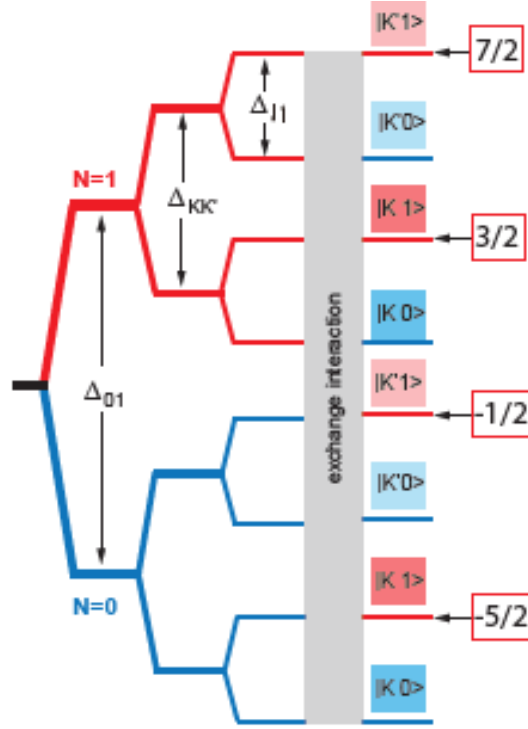


FIGURE 5.4: Single particle energy level diagram of the LLL for constant D

(BSSs) with orbital index $N = 1$. By contrast, no even denominator states appear within the $N = 0$ BSSs.

A schematic phase diagram of the ordering associated with each state is shown in figure 5.4 . Identifying the precise ground state for each BSS is difficult since interaction effects can reorder the LLs expected from a simple single particle description of degeneracy lifting.

Figure 5.5 shows traces of the longitudinal resistance and transverse conductance around $\frac{1}{2}$, and $\frac{3}{2}$ filling, acquired at fixed density n , and D , while varying B .

For $0 \leq \nu \leq 1$, the wavefunction is characterized by orbital index $N = 0$. A well developed series of FQHE states is observed, following the usual Jain sequence of composite Fermions (CFs), with the highest resolvable CF state at $\nu = \frac{4}{9}$. At half

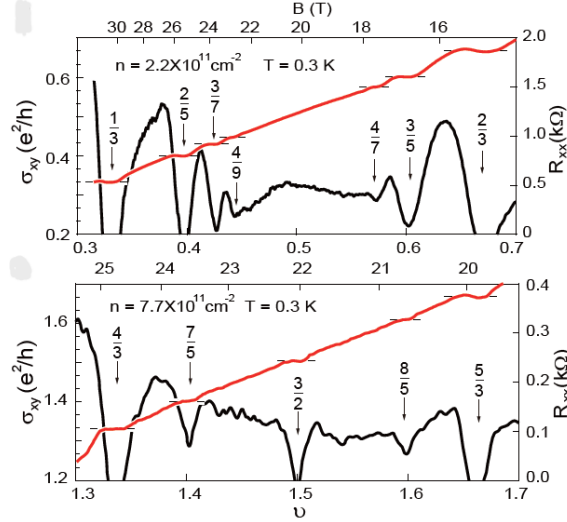


FIGURE 5.5: Shows σ_{xx} and R_{xy} acquired by sweeping B at fixed carrier densities corresponding to filling fractions spanning $0 \leq \nu \leq 1$ and $1 \leq \nu \leq 2$ respectively

filling, the longitudinal and Hall response both appear featureless. Qualitatively this sequence closely resembles the FQHE hierarchy observed in the $N = 0$ LLs in GaAs.

In stark contrast is the behaviour between $1 \leq \nu \leq 2$, corresponding to a BSS with orbital index $N = 1$. Fewer FQHE states are resolved, with only the $n=3$ CF states appearing fully developed. A robust incompressible state is clearly present at $\nu = \frac{3}{2}$, marked by zero longitudinal resistance simultaneous with a quantized Hall plateau. The qualitative similarity to the $N = 1$ states observed in GaAs and more recently in ZnO, both in terms of the even-denominator state appearing at half filling, and its strength relative to the FQHE states away from half filling, highlights the important role played by the orbital wavefunction in determining the interaction driven behavior. Moreover, the $N = 1$ orbital selection rule suggests that the even denominator FQHE observed here may be the same MR Pfaffian ground state in GaAs.

5.3 Gapped Bilayer Graphene

Our goal will be to calculate the energy gaps between even denominator states appearing at the $N = 1$ orbital index considering exchange interaction. For this it will be very important to determine the Hamiltonian matrix at valley K and K'. Although this time, we must realize that there is a potential asymmetry present at different sites of both layers. Firstly, BLG is being kept in hexagonal Boron Nitride due to which the effective coulomb interaction at site A_2 and B_2 of bottom layer will varies. Apart from that, we are also introducing electric field which introduces a potential difference between both layers. Then we are considering Zeeman splitting and exchange interaction as well. Since BLG is being kept in between top and bottom gates, this will affects the electron number density at both layers. All these will affects our Hamiltonian matrix.

To start simply, let us assume an interlayer asymmetry between the on-site energy Δ for the atoms, A_1 and B_1 , on the first layer and Δ for the atoms, A_2 and B_2 , on the second layer. The Hamiltonian matrix then becomes (in absence of Magnetic field)

$$H = \begin{bmatrix} \Delta & \nu p_- & 0 & 0 \\ \nu p_+ & \Delta & -\gamma_1 & 0 \\ 0 & -\gamma_1 & -\Delta & \nu p_- \\ 0 & 0 & \nu p_+ & -\Delta \end{bmatrix}$$

In a magnetic field, the interlayer asymmetric potential Δ causes a valley splitting of the Landau levels that is similar to monolayer graphene, since it breaks the inversion symmetry. Figure 5.6 illustrates an example of the Landau level structure in the presence of $\Delta > 0$. The two lowest levels of $(0, \pm)$, which used to be at the Dirac point when $\Delta = 0$, now move to the top of the valence band at point K, and to the bottom of the conduction band at point K'. We now use such Hamiltonian to

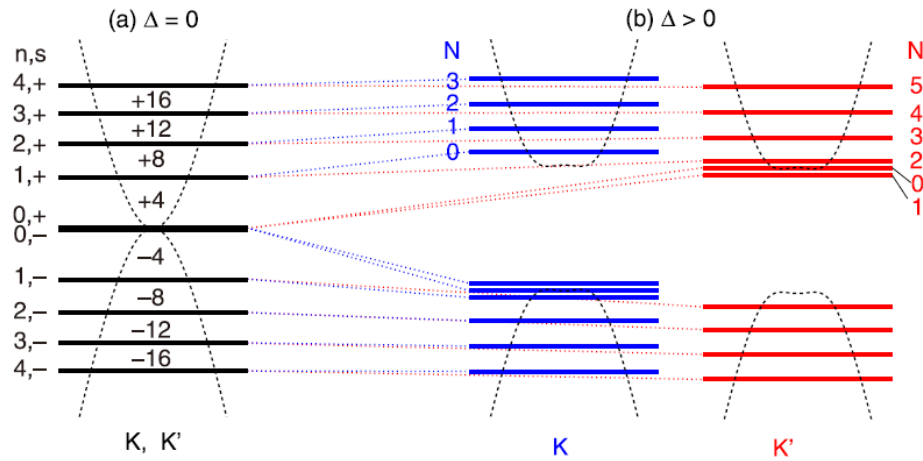


FIGURE 5.6: Low-energy Landau level structure in BLG with interlayer potential asymmetry (a) $\Delta = 0$ and (b) $\Delta > 0$

calculate energy gaps between even denominator states.

Chapter 6

Energy Gaps between even denominator states

6.1 Constructing the Hamiltonian

We recall that the Hamiltonian at valley K can be written in the form without considering magnetic fields and potential asymmetry:

$$H_K = \begin{bmatrix} 0 & \nu p_- & -\nu_4 p_- & \nu_3 p_+ \\ \nu p_+ & 0 & -\gamma_1 & -\nu_4 p_- \\ -\nu_4 p_+ & -\gamma_1 & 0 & \nu p_- \\ \nu_3 p_- & -\nu_4 p_+ & \nu p_+ & 0 \end{bmatrix}$$

In presence of magnetic field, $p_{\pm} \rightarrow \pi_{\pm}$ where $\pi_{\pm} = \pi_x \pm i\pi_y$ and $\pi_+ = \frac{\sqrt{2}\hbar}{l_B} a^{\dagger}$ and $\pi_- = \frac{\sqrt{2}\hbar}{l_B} a$. Similarly we can write Hamiltonian at K' valley by replacing π_+ with π_- and vice-versa.

Now from previous chapter, we recall that the bottom layer of BLG is being kept in hBN substrate. The hBN has dielectric constants $\epsilon_{BN}^{\perp} = 3$ in the perpendicular direction and $\epsilon_{BN}^{\parallel} = 6.6$ within the two-dimensional plane. The interaction between

electrons is the screened Coulomb potential

$$V_{SC}(q) = \frac{e^2}{4\pi\epsilon_0\epsilon_{BN}^{\parallel}l_B} \frac{2\pi}{q} \tanh qd = \frac{2\pi}{q} \tanh qd \frac{56.2}{\epsilon_{BN}^{\parallel}} \sqrt{B[Tesla]} meV$$

We need to perform fourier transform of above expression to find $V(r)$ at sites A_2 and B_2 . Apart from that, we introduce Electric field in perpendicular direction due to which there will be potential asymmetry across layers. We consider potential to be equal to $eEd/2$ at top layer and $-eEd/2$ at the bottom layer. There is also an intrinsic energy difference between the sites $B1$ and $A2$ that is Δ' . We can also consider Zeeman splitting by including $\Delta_{ZS} = g\mu_B B$. Considering everything the modified Hamiltonian that we obtain is as follows

$$H_K = \begin{bmatrix} \Delta_{ZS} + eEd/2 & \nu\pi_- & -\nu_4\pi_- & \nu_3\pi_+ \\ \nu\pi_+ & \Delta' + \Delta_{ZS} + eEd/2 & -\gamma_1 & -\nu_4\pi_- \\ -\nu_4\pi_+ & -\gamma_1 & \Delta' + \Delta_{ZS} + V_{A_2} - eEd/2 & \nu\pi_- \\ \nu_3\pi_- & -\nu_4\pi_+ & \nu\pi_+ & V_{B_2} + \Delta_{ZS} - eEd/d \end{bmatrix}$$

The eigenvalues we obtain for above Hamiltonian, corresponds to spin-up states. To get eigenvalues of spin-down states, we write $-\Delta_{ZS}$ in place of Δ_{ZS} . Similarly we can obtain Hamiltonian for K' valley by replacing $\pi_+ \rightarrow \pi_-$ and vice-versa.

6.2 Landau Level diagrams

If we focus again on figure 5.3, we find several even denominator states occuring at filling fractions $-\frac{5}{2}, -\frac{1}{2}, \frac{3}{2}$ and $\frac{7}{2}$. The range of the magnetic field is around 12-18 Tesla and $-\frac{5}{2}$ and $-\frac{1}{2}$ states were observed at Electric field, $D = -100$ mV/nm while $\frac{3}{2}$ and $\frac{7}{2}$ states were observed at $D = 35$ mV/nm. These results were observed experimentally. The set-up can be seen in figure 5.1 . Below we can observe how energy eigenvalues vary with Magnetic field (range of magnetic field taken from 12 - 18 T)

for different cases and we will see the splitting in the Landau levels on introducing Electric field and considering Zeeman splitting. While plotting Energy eigenvalues against potential due to Electric field D, we see level crossings. This signifies a lot of things which is discussed further.

Case 1 : Not considering Zeeman Splitting and Electric field D

We obtain the following plot (only showing lowest energy levels)

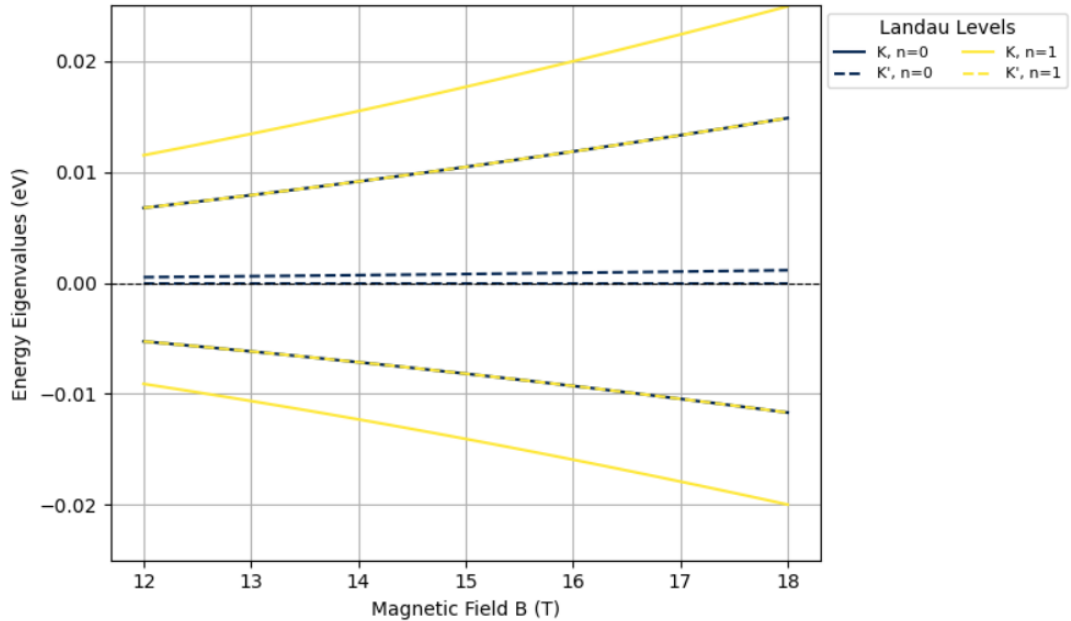


FIGURE 6.1: Energy Eigenvalues vs Magnetic Field for zero energy Landau level (ZLL) without considering Zeeman Splitting and Electric field E

The above figure can be clearly understood if I show separate plots for valley K and valley K'.

We observe that in absence of Electric field and not considering Zeeman splitting and on applying magnetic field (12-18 T) and considering Screening effects, the energy levels $|K, n = 0\rangle$ and $|K', n = 1\rangle$ overlap. Here n corresponds to Landau

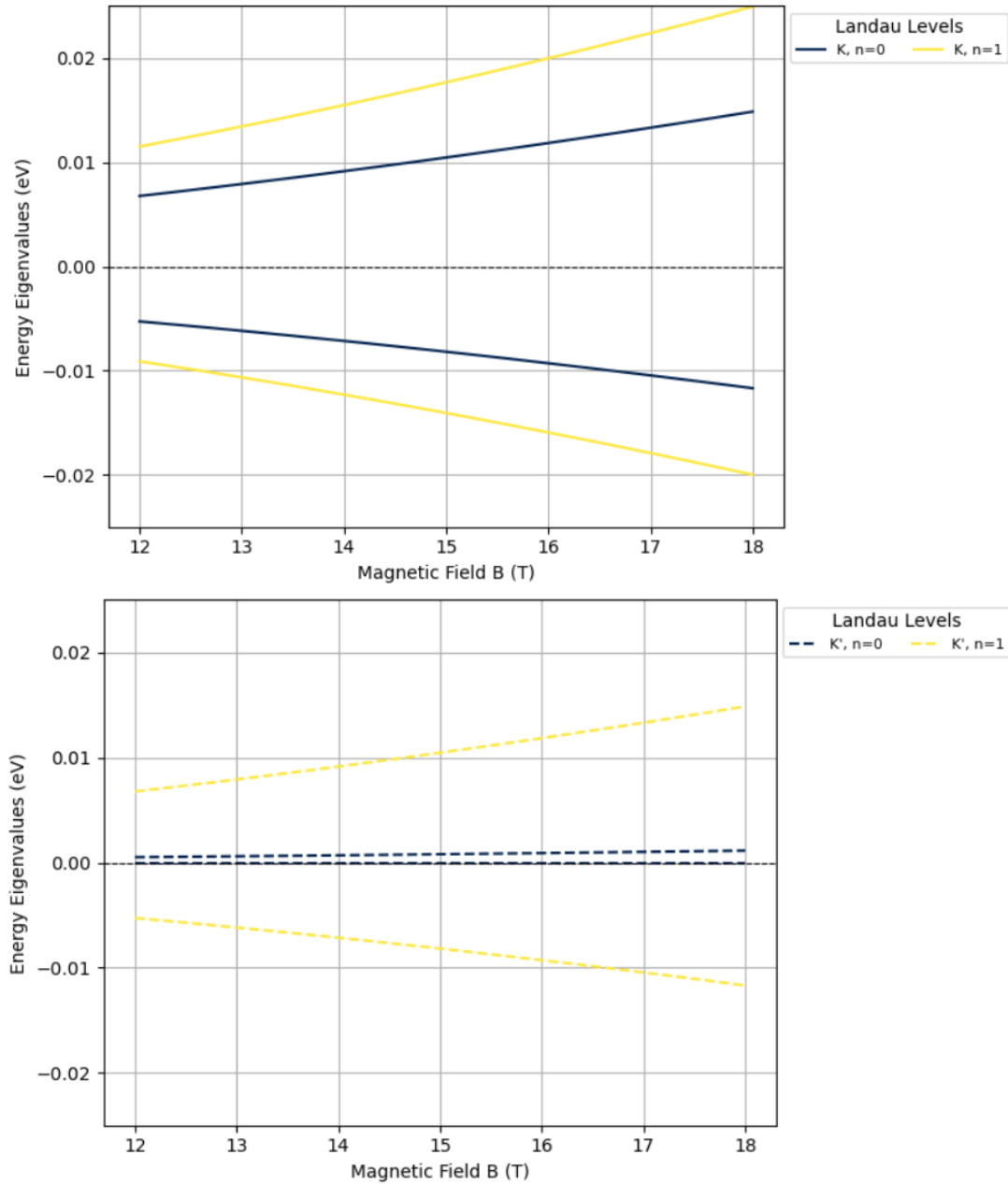


FIGURE 6.2: Energy levels for valley K and K'

level of Graphene. The LLL and $n = 1$ LL comprises a mixture of non-relativistic conventional Landau orbital 0 and 1 wavefunctions. Due to the application of magnetic field, the relative weight of the conventional 0, 1 contributions gets modified and the degeneracy gets lifted. In figure 6.2, we observe 2 lines for each $|K, n\rangle$ state. This corresponds to different conventional Landau orbital.

Case 2: Considering Zeeman Splitting but not Electric field

We obtain the following plot

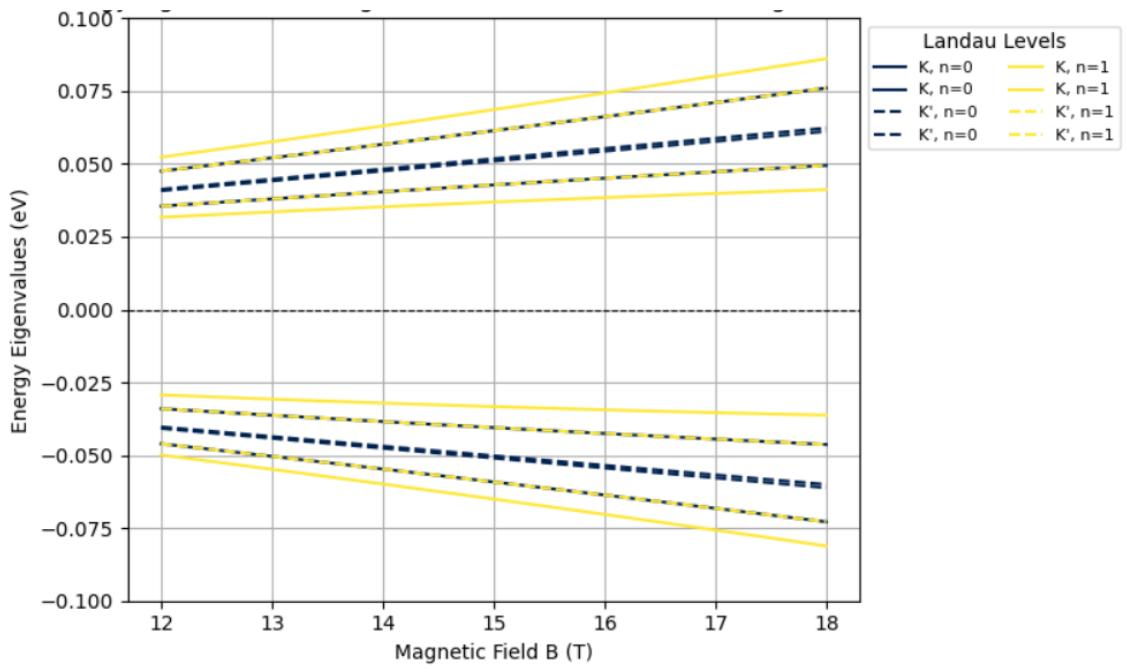


FIGURE 6.3: Energy Eigenvalues vs Magnetic Field for $n = 0, 1$ considering Zeeman Splitting but not Electric field

The above figure can be clearly understood if again I focus on separate plots for valley K and valley K' (figure 6.4).

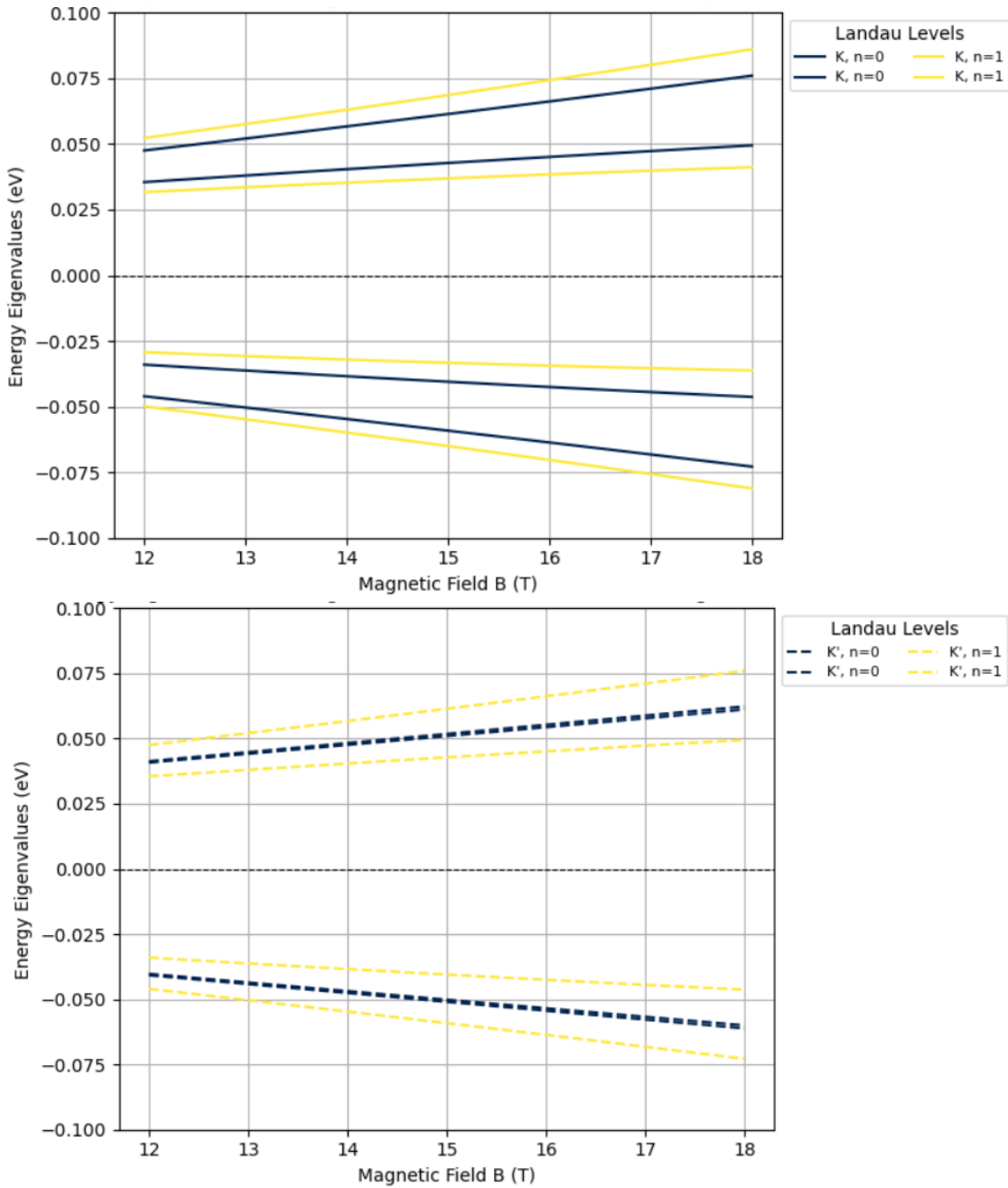


FIGURE 6.4: Energy levels for valley K and K'

Focus on figure 6.2 and figure 6.4 . Firstly observe plots for valley K. In figure 6.2, we observe 2 lines each for $|K, 0\rangle$ and $|K, 1\rangle$ each corresponding to conventional Landau orbitals 0 and 1. But in figure 6.4, there are 4 lines each for $|K, 0\rangle$ and $|K, 1\rangle$ or in other words 2 lines each for a typical state $|\xi, N, n\rangle$ where ξ corresponds to valley K or K', N corresponds to Landau level of Graphene and n corresponds to conventional Landau orbital 0 or 1. These 2 lines for each of the $|K, 0, 0\rangle$, $|K, 0, 1\rangle$, $|K, 1, 0\rangle$ and $|K, 1, 1\rangle$ states corresponds to spin up and spin down states. Same comments can be said for $|K', N, n\rangle$ states as well.

You may take a look at figure 6.5 as well which separately shows the splitting of each state into spin-up and spin-down states.

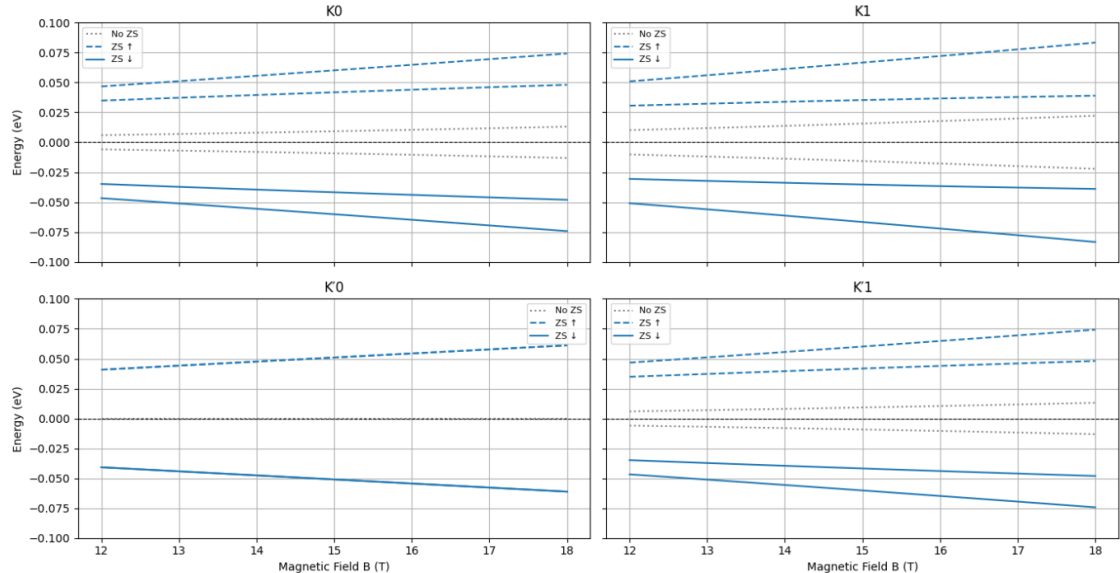


FIGURE 6.5: Landau Level Evolution for K0, K1, K0, K1 — with/without Zeeman Splitting

Case 3: Now considering both Zeeman Splitting and Electric field E

The below plots will show the variation of energy eigenvalues with Magnetic field keeping Electric field fixed. The constant Electric field considered here is 35 mV/nm.

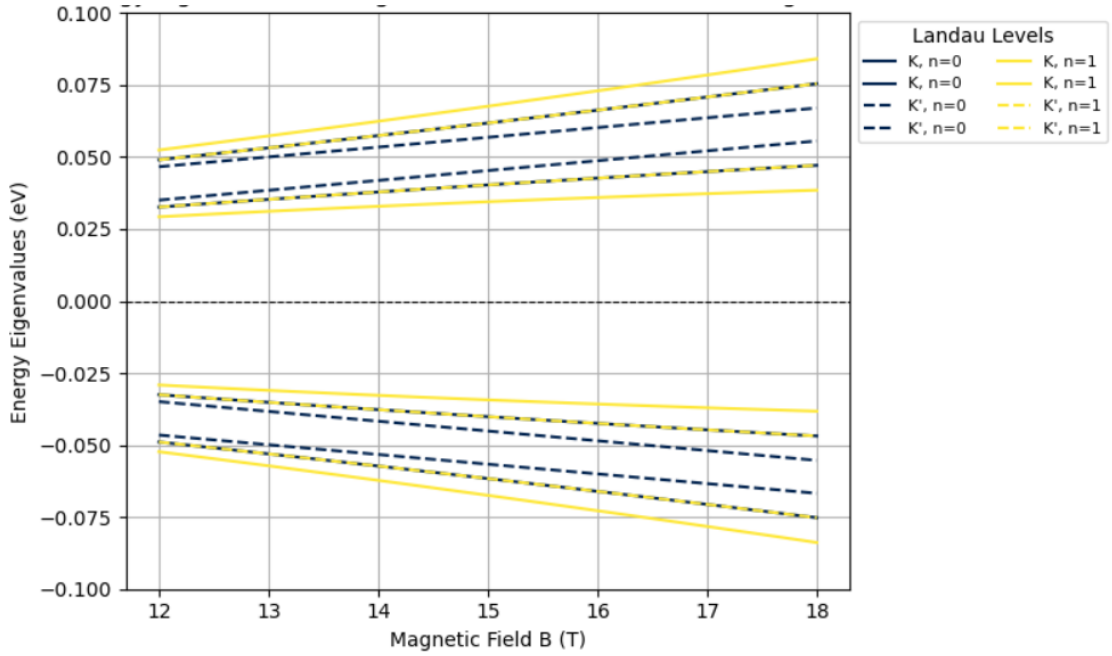


FIGURE 6.6: Energy Eigenvalues vs Magnetic Field for $n = 0, 1$ considering both Zeeman Splitting and Electric field

Again focussing on separate plots for valley K and valley K' (figure 6.7).

Applying a transverse electric field, E , breaks the inversion symmetry between the two sets of graphene lattices and induces phase transitions between ground states with different valley and orbital polarizations. The application of both B and D fields therefore makes it theoretically possible to dynamically tune several key parameters within a single device, including the orbital wave function, effective Coulomb interaction, and LL mixing. Optimizing these parameters in BLG is predicted to yield a more robust even denominator state than that in GaAs.

Figure 6.8 separately shows the Landau level spectrum in all above cases for every possible state $|\xi, N, n\rangle$.

There is energy difference for all possible states by introducing Electric field, although the difference doesn't appear much. We can also plot the Energy eigenvalues

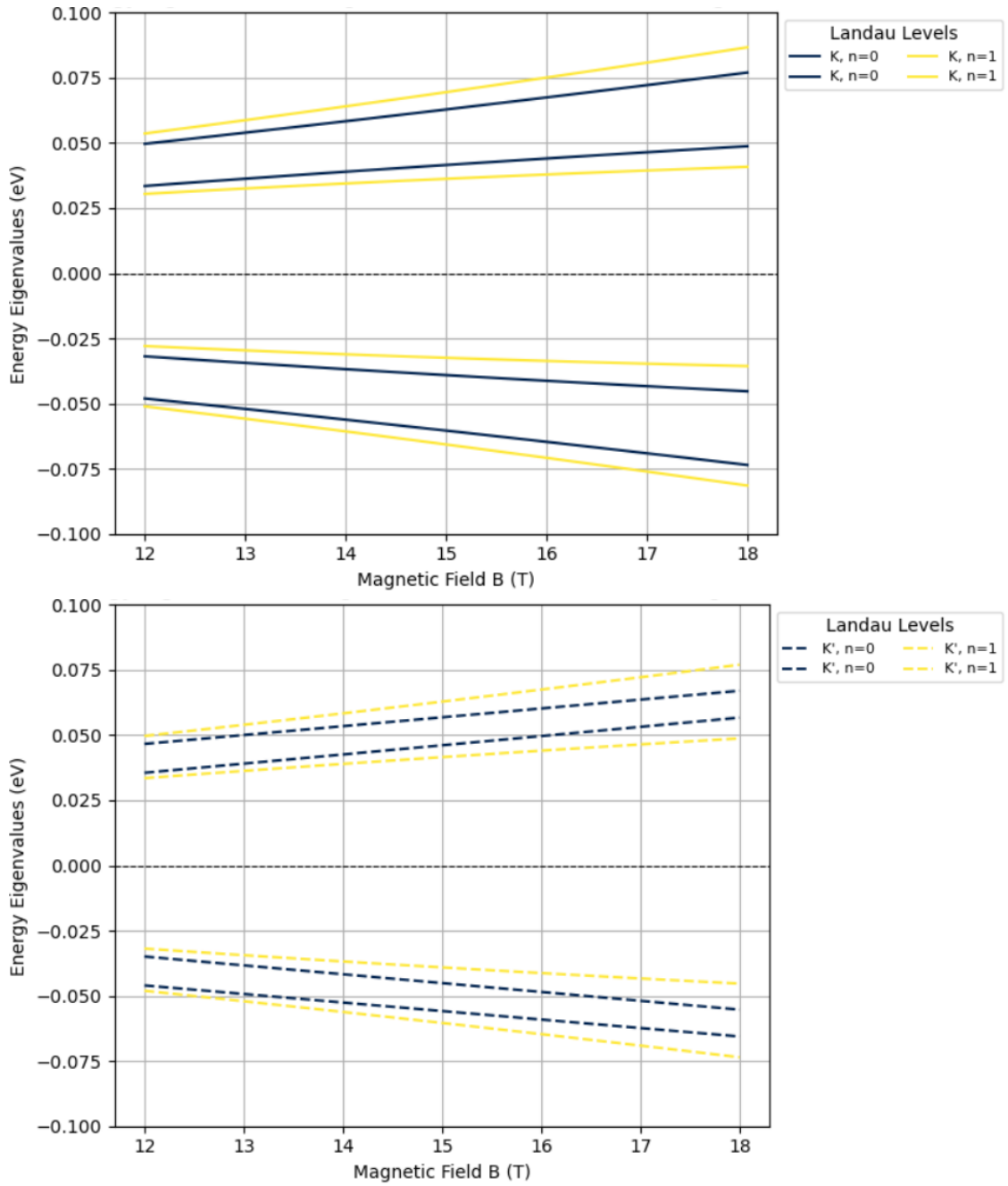


FIGURE 6.7: Energy levels for valley K and K'

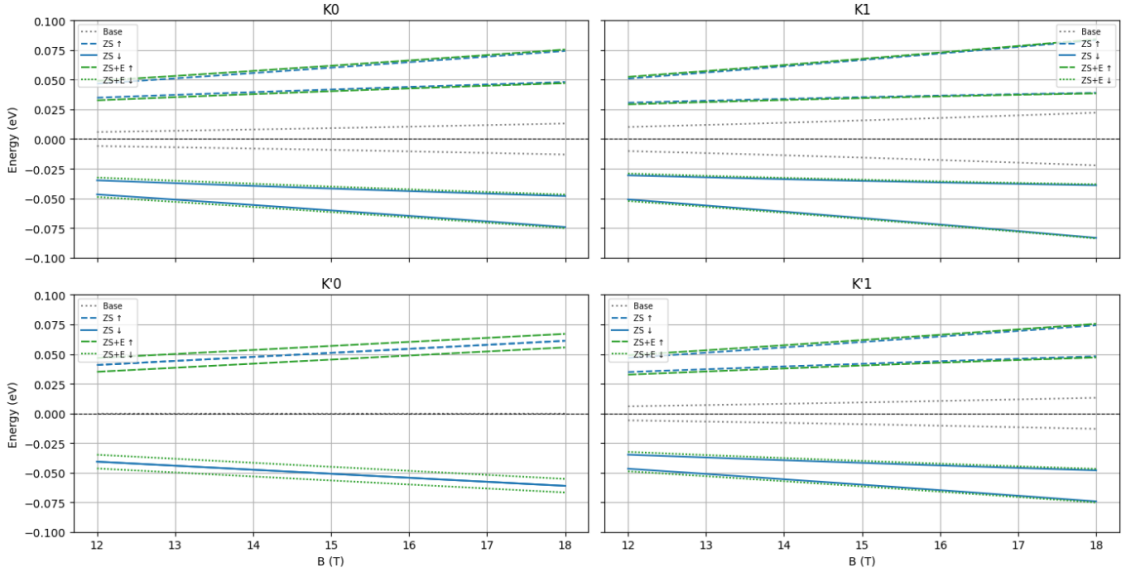


FIGURE 6.8: Landau Level Comparison for K0, K1, K'0, K'1 — ZS vs ZS + E vs Base(No ZS and No E)

against the potential difference due to Electric field. The plot has been shown in figure 6.9. We observe level crossing near Potential difference at 0 meV (not exactly at 0 meV). The level crossings signifies phase transition between different ground states, especially in systems with interactions. The system may switch between spin-polarized, layer-polarized, or valley-polarized ground states. This is particularly important for even-denominator FQHE states where the order of pseudospin levels (e.g., layer, spin, valley) matters.

To understand figure 6.9, we can again separately focus on plots for valley K and K' which is shown in figure 6.10.

We can observe level crossing for valley K', n = 0 and spin down states which indicates some sort of phase transitions between conventional non-relativistic landau orbitals 0 and 1 near Potential difference at 0 meV. These level crossings can also be observed when we do plotting of energy eigenvalues against magnetic field for a

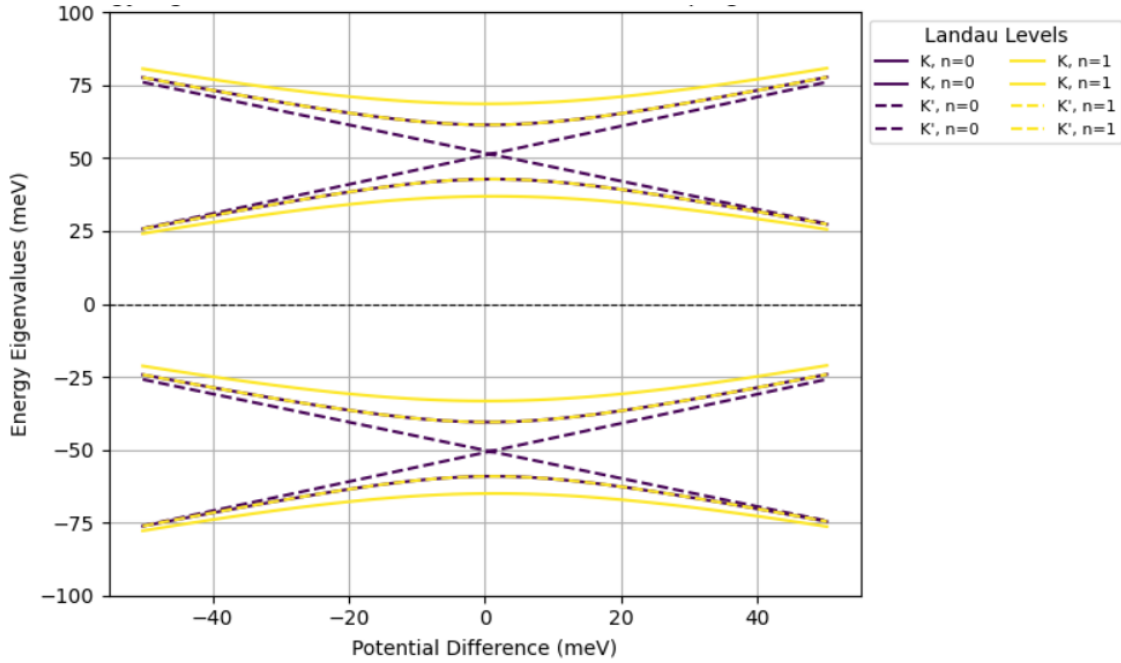


FIGURE 6.9: Energy Eigenvalues vs Electric Field for $n = 0, 1$ keeping B fixed at 15T

constant Electric field value.

Recall that the $\frac{3}{2}$ and $\frac{7}{2}$ states occur at $E = 35$ mV/nm where the magnetic field range is 12-18 T. Similarly, we can observe the states $-\frac{5}{2}$ and $-\frac{1}{2}$ at $E = -100$ mV/nm. We can plot Landau level diagrams for $E_1 = -100$ mV/nm (labeled as set-1) and $E_2 = 35$ mV/nm (labeled as set-2). The plot can be seen in figure 6.11 .

Indeed the plot is really messy. We therefore focus on some particular landau levels to observe where landau levels crossing exactly happens.

Part 1 : Observing separate Landau levels occurring at $E = -100$ mV/nm and $E = 35$ mV/nm:

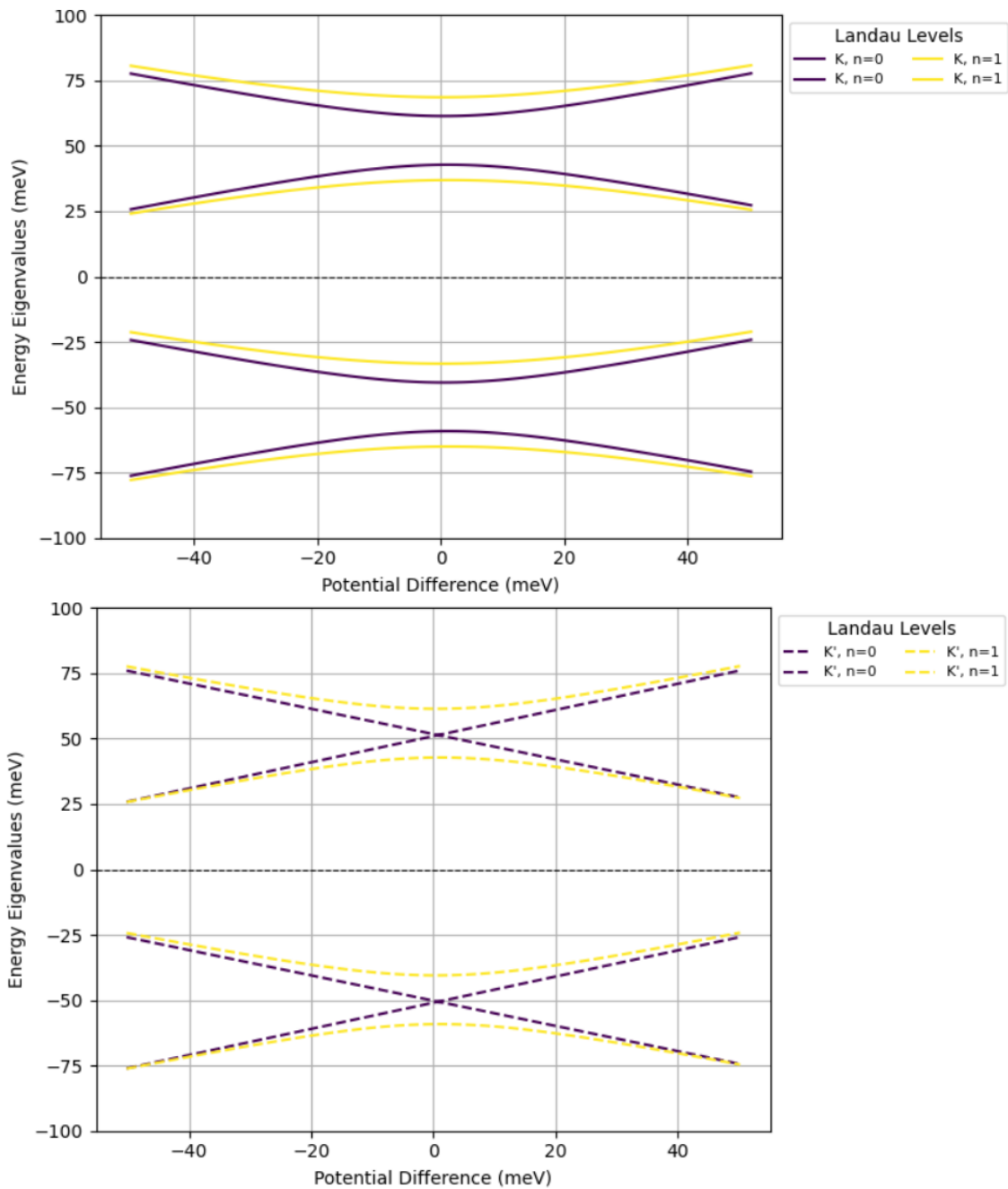


FIGURE 6.10: Plots for valley K and K'

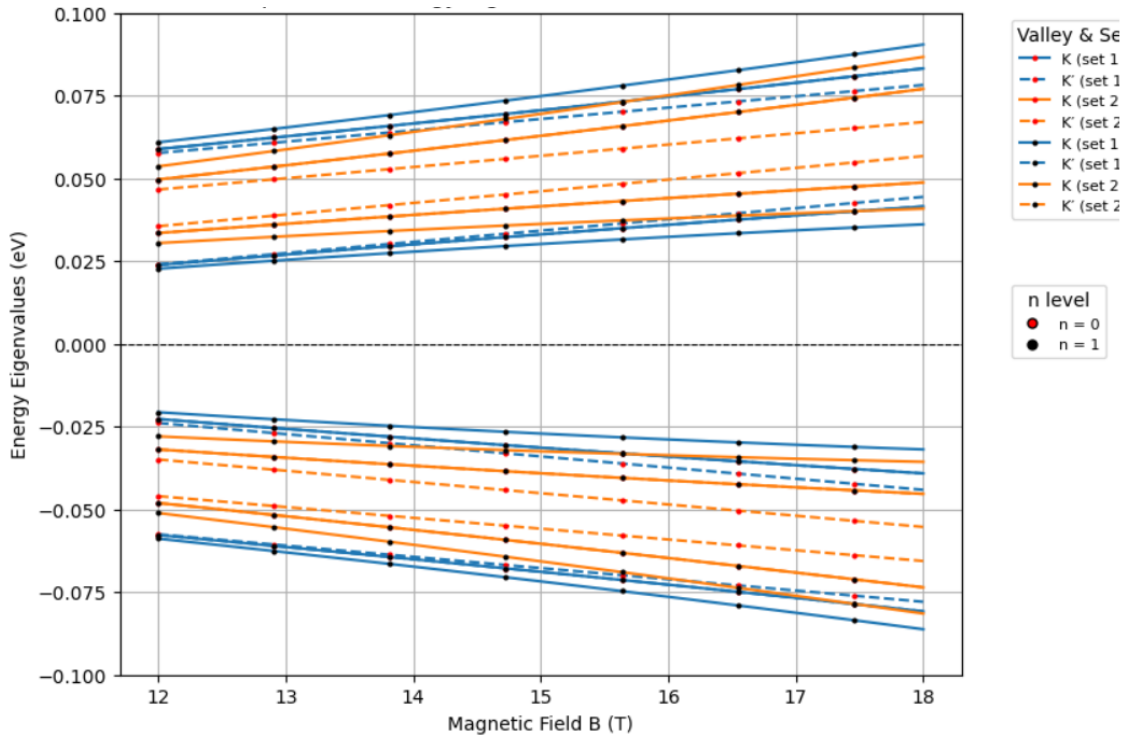


FIGURE 6.11: Comparison of Energy Eigenvalues (ZS + E): Set 1 vs Set 2

There does not occur any Landau level crossing which indicates that no transition occurs between states $-\frac{5}{2}$ and $-\frac{1}{2}$ and between states $\frac{3}{2}$ and $\frac{7}{2}$.

This will be explained more at the end of this section.

Part 2 : Observing separate Landau levels of valley K and K':

We observe that there is no Landau level crossing of states corresponding to valley K' but there occurs Landau level crossings of states corresponding to valley K. The level corresponding to valley K and n=1 (set 2) crosses with level corresponding to valley K and n=0 at (set 1) at magnetic field between 17 T and 18 T. The same level crossing also occurs between 15 T and 16 T (close to 16 T). It occurs for both negative and positive energy eigenvalues.

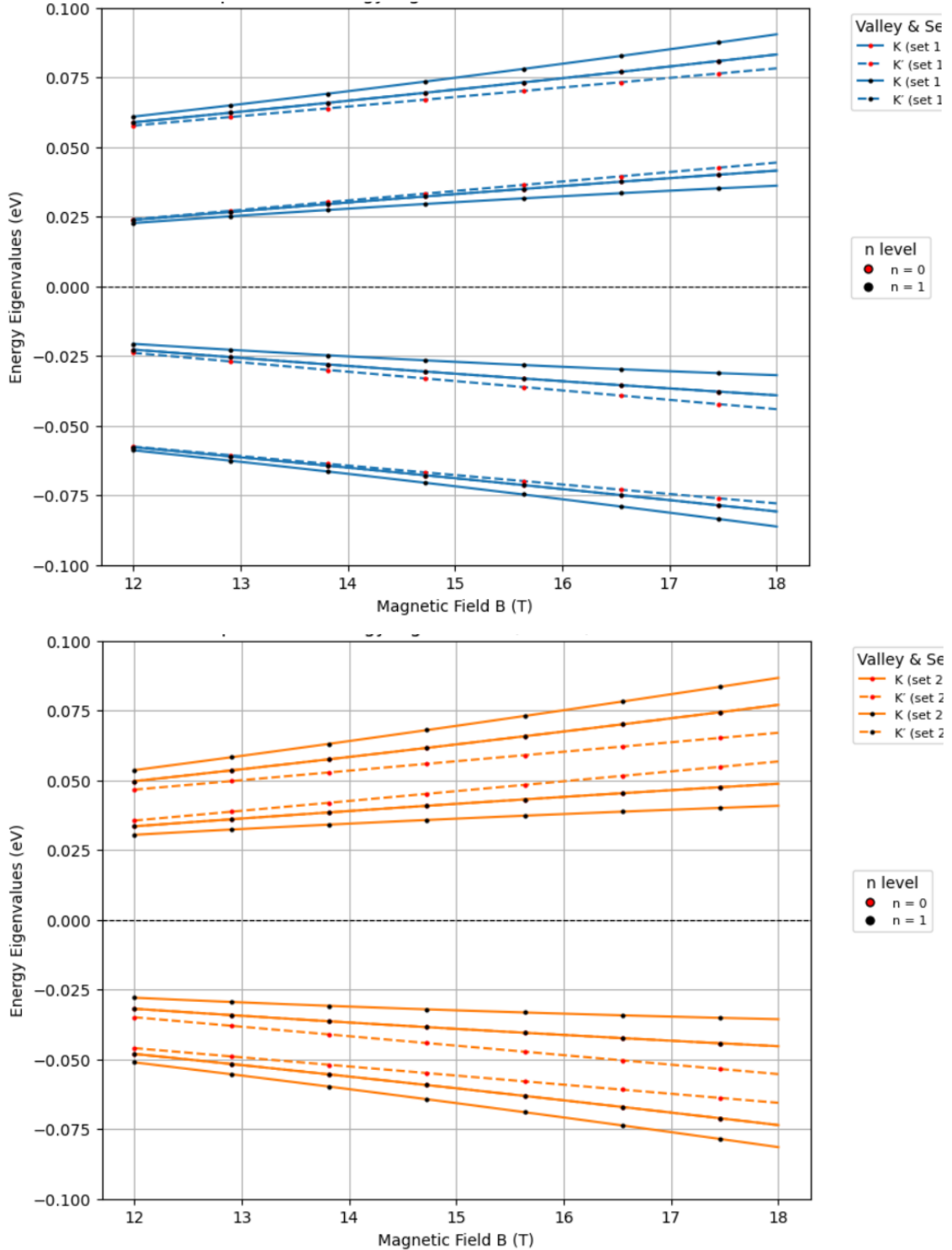


FIGURE 6.12: Landau levels at $E = -100\text{mV/nm}$ (up) and $E = 35\text{ mV/nm}$ (down)

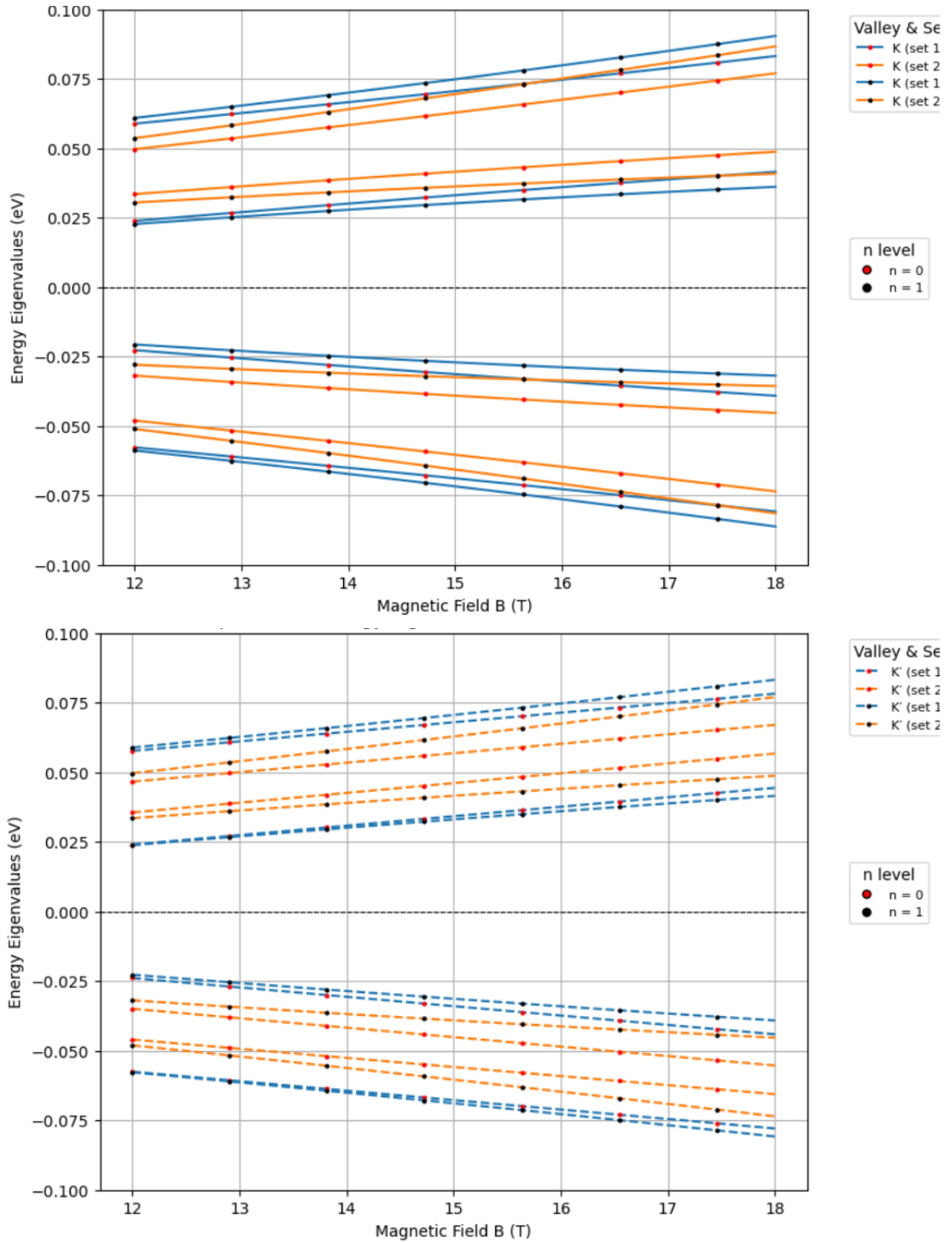


FIGURE 6.13: Landau levels of valley K (up) and valley K'(down)

Part 3 : Observing separate Landau levels for spin-up and spin-down states:

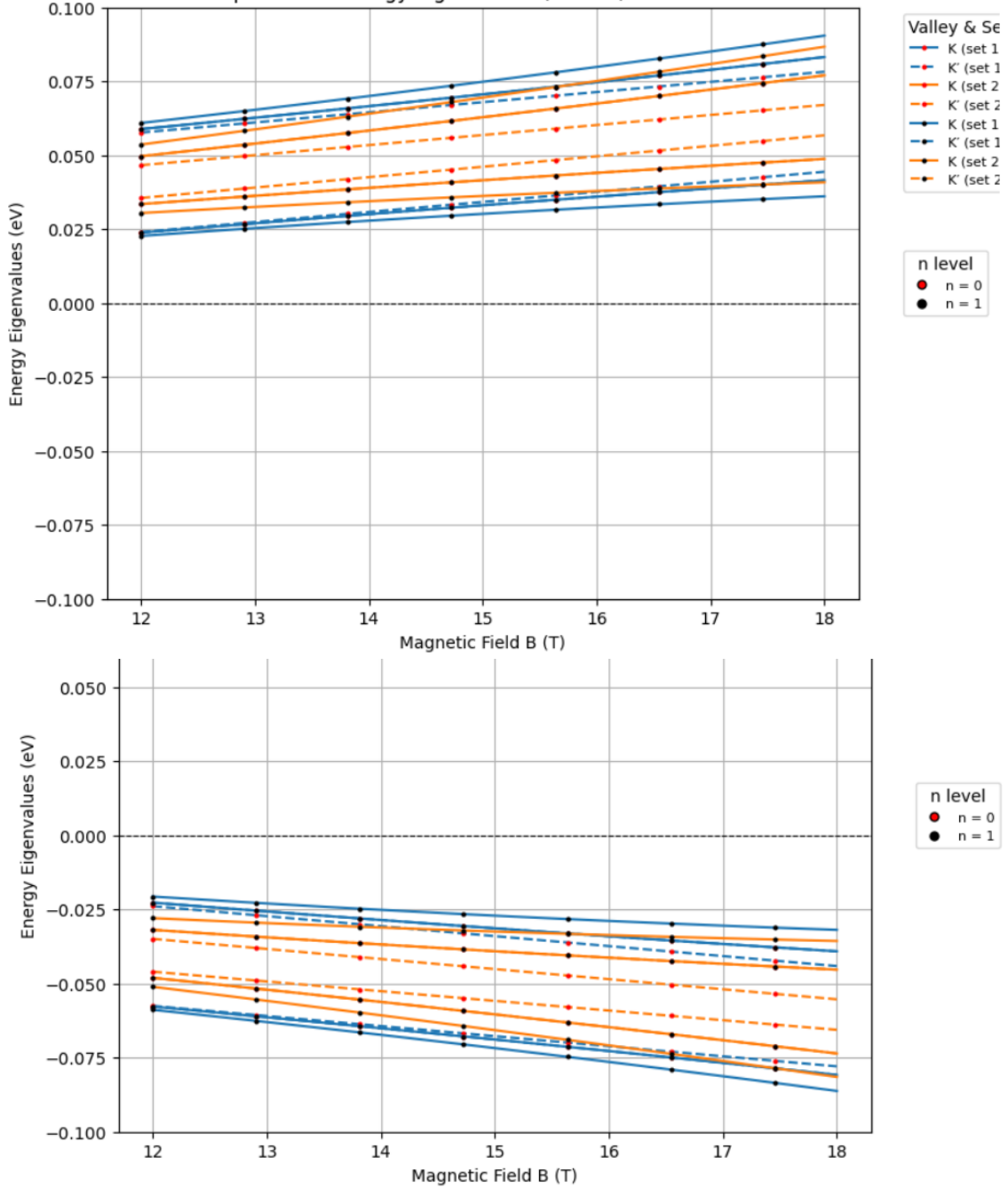


FIGURE 6.14: Landau levels of spin-up (up) and spin-down (down) states

For spin-up states, we observe that the Landau level corresponding to valley K and $n = 1$ (set 2) crosses with level corresponding to valley K' and $n = 0$ (set 1) at

magnetic field, close to 16 T (between 16 T and 17 T) and then with valley K and $n = 1$ (set 1) at magnetic field between 17T and 18T. This same level crossings also occur at magnetic field between 14T and 15T (level crossing with valley K', $n = 0$, set 1) and at magnetic field between 15T and 16T (level crossing with valley K, $n = 1$, set 1). This same phenomena will be observed for spin-down states as well.

Case 4: Now considering Exchange Interaction :

The Pauli Exclusion principle is a result of a more fundamental thing, namely fermion antisymmetry. If we have a wave function that describes two fermions $\Psi(r_1, r_2)$, where r_1 and r_2 are the coordinates of the two fermions, then it has to be antisymmetric (change sign) when the particles are exchanged. In other words $\Psi(r_1, r_2) = -\Psi(r_2, r_1)$.

If we do the math on this, we'll find that two fermions with the same spin cannot exist in the same energy state (in the case of electrons: orbital), because the total wave function becomes zero, which is an invalid result. This isn't part of the Schrödinger equation itself, it's a boundary condition we have to apply for it to be correct, like the normalization condition. But that doesn't stop us from trying. So in its most general form, the 'exchange energy' amounts to the difference in energy between the system where we satisfied the antisymmetry condition and one where we didn't.

Strictly speaking it's not an interaction. There's no exchange particle, there's no term in the original Hamiltonian that represents it. The way it comes into play is the Hartree-Fock method. That's an approximate way of solving the difficult quantum many-body problem, by treating each electron so that it only interacts with the mean field of every other electron. (so it's also known as the 'mean field approach') In that approach it's easy to satisfy the antisymmetry condition; we create a wave

function that's a so-called Slater determinant; a linear product of the various electronic orbitals that satisfies the antisymmetry condition.

So when we stick our Slater determinant wave function in the mean-field Hamiltonian, and do some work, we end up with the "Fock operator", which is basically the Hamiltonian within this approximation. It consists of a term for the electronic kinetic energy, the electron-nuclear potential energy, the electron-electron repulsion and an additional term that came about from using the Slater determinant (i.e. antisymmetry). That's the 'exchange operator', which we could view as describing this 'exchange interaction'.

Here we are not considering all of this. We have simply taken the exchange interaction to be a constant, that is $J_{ex} = 32\text{meV}$ which was calculated for AB stacked Bilayer Graphene with bottom layer inside hBN substrate. Below we will see how the LL spectrum will change on considering exchange interaction.

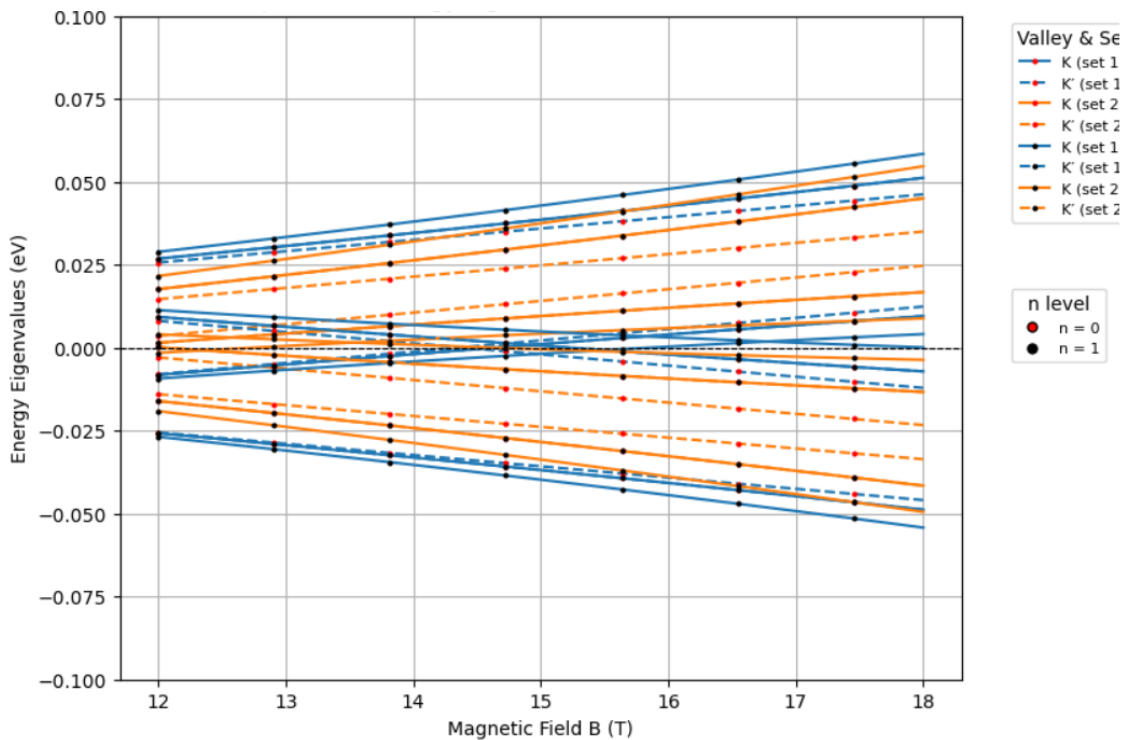


FIGURE 6.15: Comparision of Energy eigenvalues ($ZS + E + J_{ex}$)

Figure 6.15 shows the LL spectrum on considering exchange interaction. Comparing it with figure 6.11, we could see the difference. Again the plot is not very clear and we analyze the plot by focussing on some specific LLs based on its valley and spin.

Part 1 : Observing separate Landau levels occurring at $E = -100\text{mV/nm}$ and $E = 35\text{mV/nm}$:

Here we do observe level crossings for both LLs at $E = -100\text{ mV/nm}$ and at $E = 35\text{mV/nm}$. That means at some particular magnetic fields, transition of $-\frac{5}{2}$ to $-\frac{1}{2}$ FQH states and transition of $\frac{3}{2}$ to $\frac{7}{2}$ FQH states are possible. In the left figure, there are 2 LL with valley K and $n = 1$ (LL of BLG) and since the levels are tilted downwards, it implies that they are spin down states. These LLs are crossing with 2 LL of same valley K and $n = 1$ but with spin up (since they are tilted upwards) states and both having conventional Landau orbital either 0 or 1, and a LL of valley K', $n = 0$ (LL of BLG) and spin up state (although the conventional Landau orbital could be either 0 or 1). There is one more LL with valley K', $n = 0$ and spin down state (conventional Landau orbital could be either 0 or 1) which is crossing with the same above 3 LLs.

From the right figure, we observe a LL with valley K, $n = 1$ and spin down state, crossing with 2 LLs with valley K, $n = 1$ and spin-up states (having conventional Landau orbitals 0 and 1) and valley K', $n = 0$ and spin-up states (conventional Landau orbital either 0 or 1). There is one more LL with valley K, $n = 1$ and spin-down state crossing with valley K, $n = 1$ and spin-up state.

Part 2 :Observing separate Landau levels of valley K and K':

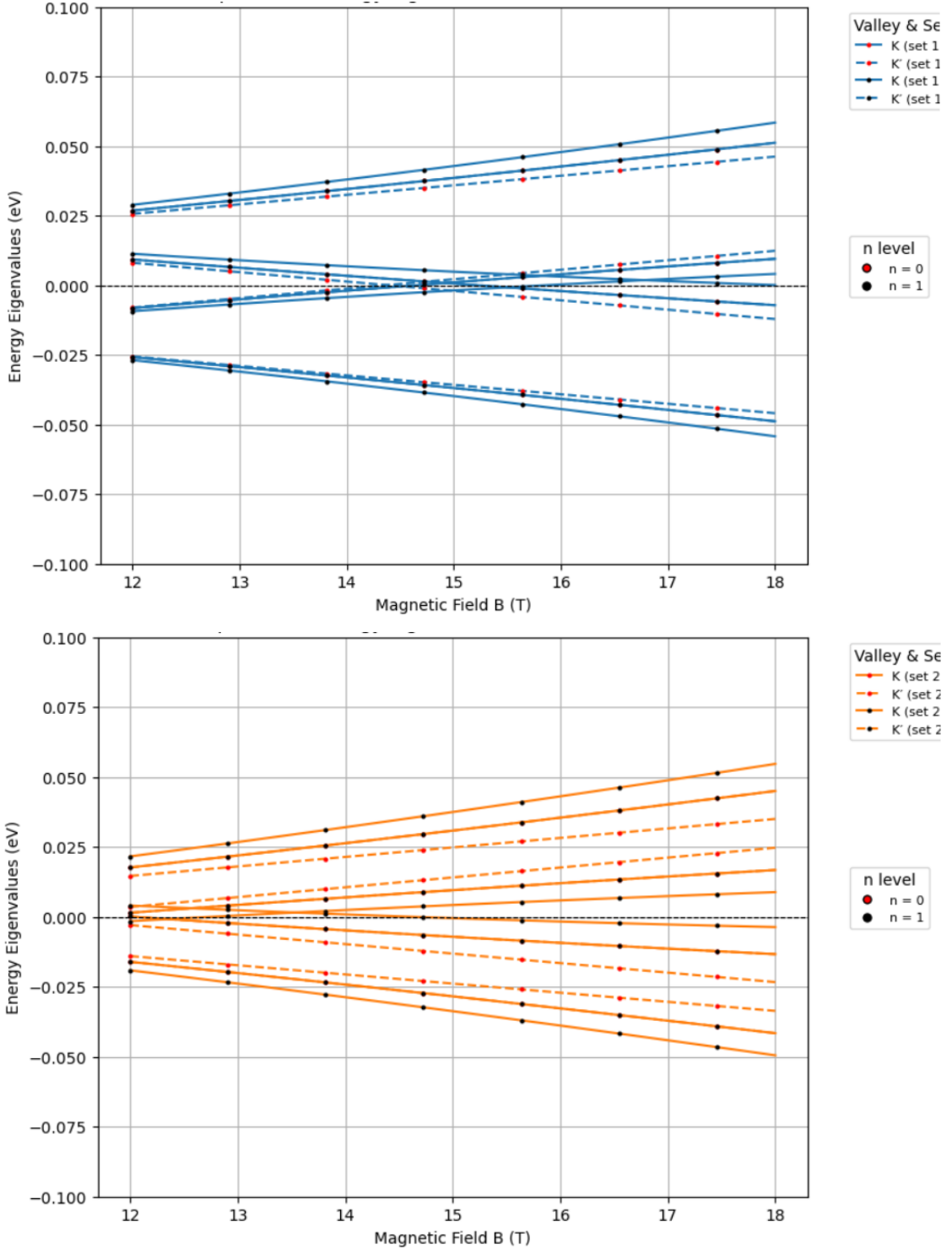


FIGURE 6.16: Landau levels at $E = -100\text{mV/nm}$ (up) and $E = 35\text{ mV/nm}$ (down) considering J_{ex}

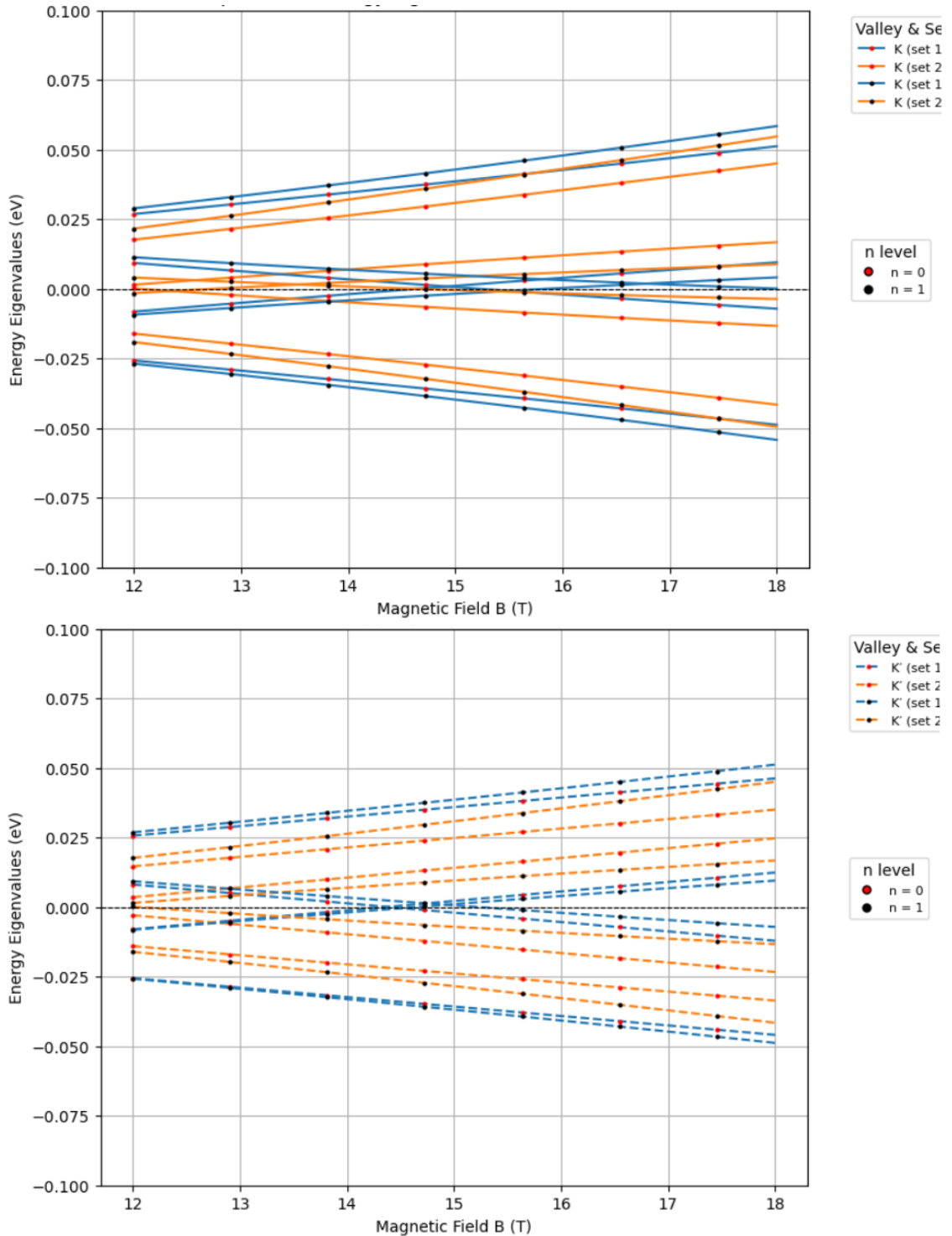


FIGURE 6.17: Landau levels of valley K (up) and valley K'(down) considering J_{ex}

In both diagrams, we can observe Level crossing. In the left diagram, there is a K valley of set 2 ($E = 35 \text{ mV/nm}$), $n = 1$ (LL of BLG) and spin down state which is crossing with valley K of set 1 ($E = -100 \text{ mV/nm}$), $n = 0$ and spin down state. The same is observed for spin up states as well. Near 0 energy eigenvalue, we find that there are 2 LLs from set 1, valley K ,spin down and both $n = 0$ and $n = 1$, which are crossing with 2 LLs of set 1 and 2 LLs of set 2,both having valley K , spin up and both $n = 0$ and $n = 1$. There are 2 LLs of set 2 as well, both having valley K, spin down and $n = 0$ and $n = 1$ which are crossing with 4 spin up, valley K states, 2 of them having $n = 0$ and other 2 having $n = 1$ LL of BLG. Near 0 energy eigenvalue, we can comment the same thing for the right figure as well for K' valley but only for those LLs from set 1. From set 2 LLs (valley K', $n = 0,1$ and spin down states), there are level crossings with both LLs from set 1, valley K', $n = 0$ and $n = 1$ and both having spin up states.

Part 3 : Observing separate Landau levels for spin-up and spin-down states:

From left figure, we find that 2 LLs, each having valley K, $n = 1$, spin up states and of set 2 (having different conventional Landau orbitals) are crossing with LLs of set 1, one having valley K, $n = 1$ and spin up states, and other having valley K', $n = 0$ and spin up states (conventional Landau orbital could be either 0 or 1). The same comment can be said from right figure as well for spin down states.

Figure 6.19 shows LL spectrum against Potential difference due to electric field. We can also observe level crossings here as well which indicates the different possible phase transitions that can take place between different possible even denominator states at some specific values of Potential difference.

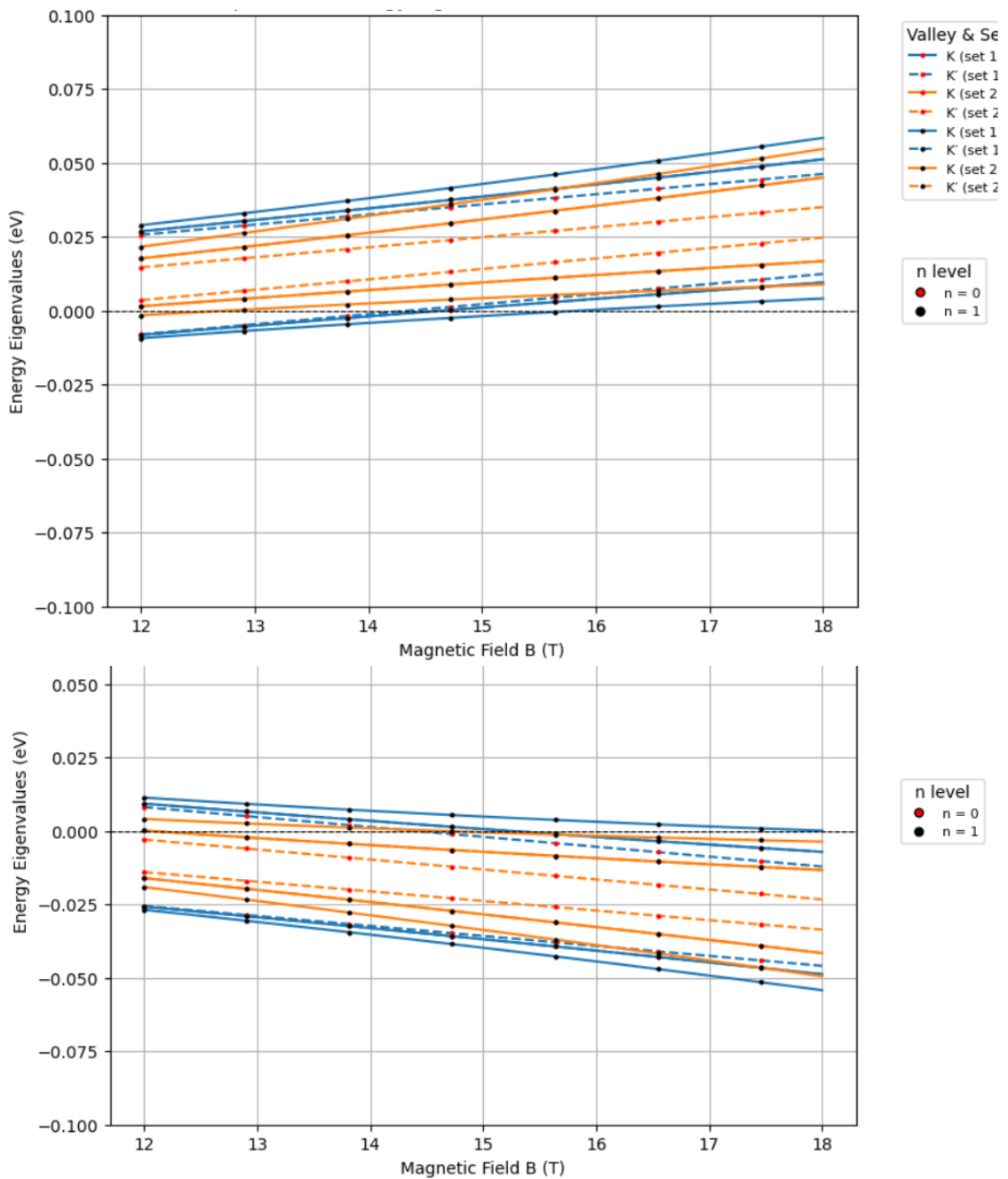


FIGURE 6.18: Landau levels of spin-up (up) and spin-down(down) states

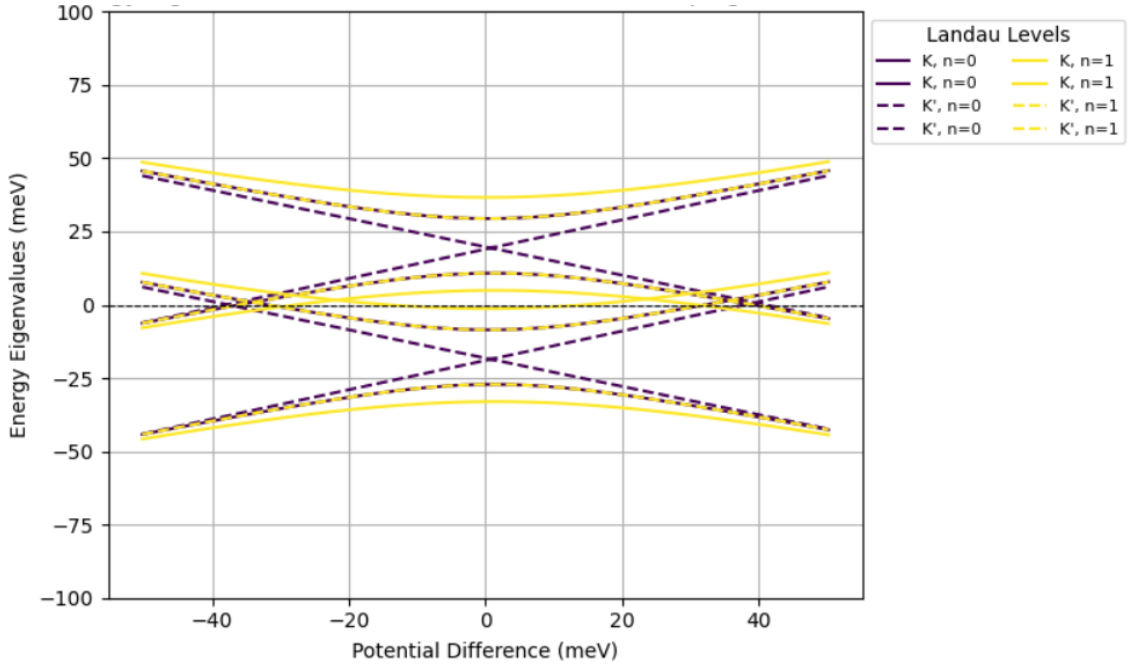


FIGURE 6.19: LL spectrum against Potential difference due to electric field considering J_{ex}

Focus on figure 6.20. This is basically the zoomed image of figure 6.15. We are specifically focussing on Landau levels close to 0 energy eigenvalue.

The LL spectrum with orange mark indicates that $E = 35\text{mV/nm}$. At $E = 35\text{ mV/nm}$ and magnetic field B in the range of 12-18 T, we observe $\frac{3}{2}$ and $\frac{7}{2}$ fractional quantum hall states. We focus on LLs with positive energy. For $\frac{3}{2}$ state to occur, the LLL (with lowest ground state energy) should be completely filled and the first excited LL should be half filled. From figure 6.20, we can observe that the LL with valley K, $n = 1$ (LL of BLG) and spin up state (conventional Landau orbital could be 0 or 1) has the lowest positive energy and hence this should be completely filled. Now the second lowest positive energy is the LL with valley K', $n = 0$ and spin-up state (conventional Landau orbital could be 0 or 1) which should be half filled to observe $\frac{3}{2}$ state. It is now understandable that to observe $\frac{7}{2}$ fractional quantum hall state, the 3 lowest landau levels that is one of valley K , $n = 1$, spin up state and

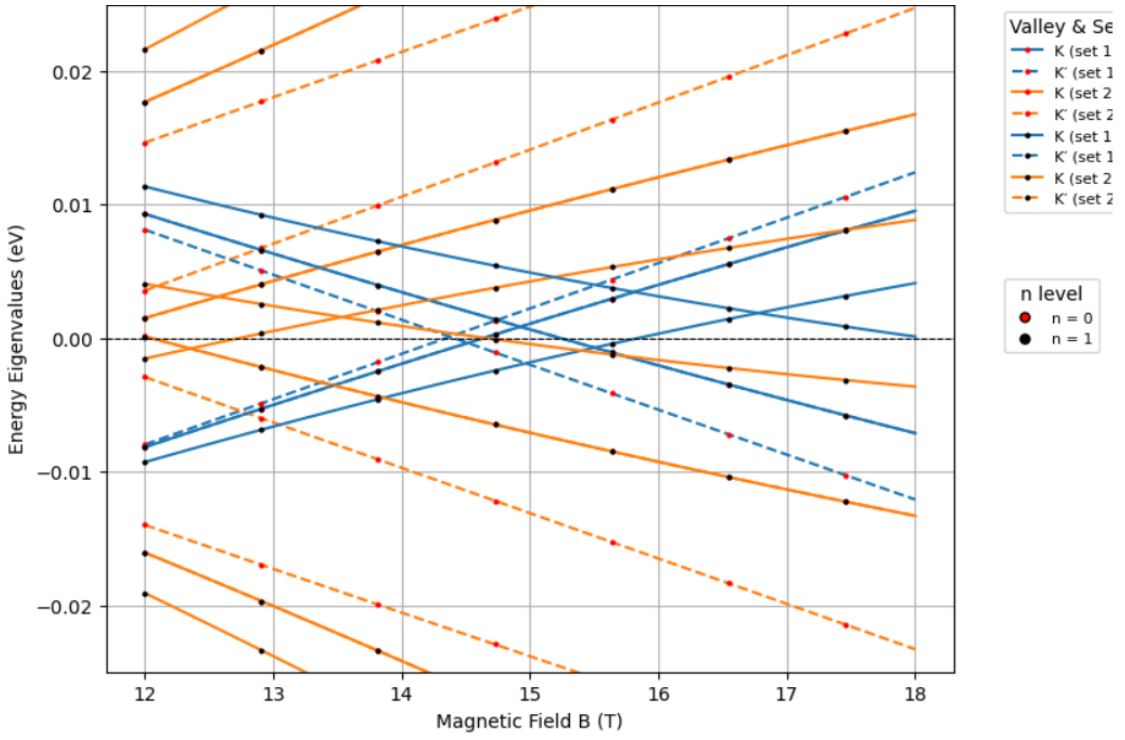


FIGURE 6.20: LL spectrum against Magnetic field near 0 energy considering J_{ex}

2 of valley K' , $n = 0$, spin up states (one having conventional Landau orbital 0 and other having conventional Landau orbital 1) should be completely filled and then a LL of valley K , $n = 1$, spin up state (but with different conventional Landau orbital compare to the previous LL of lowest energy) should be half-filled.

To observe Fractional quantum hall states $-\frac{5}{2}$ and $-\frac{1}{2}$, we shift our focus to LLs which are marked with blue which indicates that $E = -100$ mV/nm. At $E = -100$ mV/nm and magnetic field B in the range of 12-18 T, we observe $-\frac{5}{2}$ and $-\frac{1}{2}$ fractional quantum hall states. We will focus on LLs with negative energy. From figure 6.20, we observe that below $B \approx 14 - 15$ T, to observe $-\frac{1}{2}$ state, the LL with valley K' , $n = 0$ and spin up state (conventional Landau orbital could be 0 or 1) should be half filled and to observe $-\frac{5}{2}$ state, LL with valley K' , $n = 0$, spin-up state and LL with valley K , $n = 1$, spin-up state should be completely filled and the same LL with valley K , $n = 1$, spin-up state (but with different conventional Landau orbital)

should be half-filled. At around $B \approx 14 - 15\text{T}$, there are level crossings taking place, and so above $B \approx 15\text{T}$, we observe only 2 LLs, marked with blue and energy near 0. Hence we will not find $-\frac{5}{2}$ state since we require 2 fully filled LLs and 1 half-filled LL. There is no LL available near 0 energy which can be half filled. But we can observe $-\frac{1}{2}$ state. The LL with valley K, $n = 1$, spin down state (conventional orbital could be either 0 or 1) should be half filled. At some specific magnetic fields, we do observe transition between different even denominator FQH states.

We can also do similar analysis by looking at figure 6.19 . We can identify which specific LL should be fully filled or half filled and what fractional quantum hall states do we observe for a particular range of Electric field. We can also identify transitions between different even denominator fractional quantum hall states that we observe on some specific values of Electric field.

6.3 Conclusion

An important question remains: what is the ground state wavefunction of the even denominator state? A frequently considered alternative to the MR Pfaffian is the Halperin (331), an Abelian ground state resulting from a spin singlet (or possibly also valley-isospin singlet) pairing of electrons. This state however was theoretically found to be unstable in BLG, except for narrowly constrained conditions, and therefore unlikely to explain the wide ranging phase space that we observe. We consider a valley singlet pairing unlikely since we observe the even-denominator state to persist to high Electric field, where the state is assumed to be fully valley polarized. In addition to the Pfaffian, similar non-abelian ground states such as its particle-hole conjugate, the anti-Pfaffian, may be possible, depending on the strength of LL

mixing. Interestingly, the ability to tune the degree of LL mixing in graphene could make it possible to dynamically transition between the Pfaffian and anti-Pfaffian, which are topologically distinct ground states.

Bibliography

- [1] Zala Lenarcic *Landau Levels in Graphene*
- [2] David Tong *Lecture notes on Quantum Hall Effect*
- [3] Z. Papic, R.Thomale and D. A. Abanin *Tunable Electron Interactions and Fractional Quantum Hall States in Graphene*
- [4] T. Chakraborty *Physics of Graphene*
- [5] Vadim M. Apalkov, T. Chakraborty *Fractional Quantum Hall States of Dirac Electrons in Graphenes*
- [6] A.H. Castro Neto, F. Guinea, N. M. R. Peres, K. S. Novoselov and A. K. Geim *The electronic properties of Graphene*
- [7] J.I.A. Li, C.Tan, S.Chen, Y.Zeng, T.Taniguchi, K.Watanabe, J. Hone, C.R. Dean *Supplementary Material for Even denominator fractional quantum Hall states in bilayer graphene*
- [8] J.I.A. Li, C.Tan, S.Chen, Y.Zeng, T.Taniguchi, K.Watanabe, J. Hone, C.R. Dean *Even-denominator fractional quantum Hall states in bilayer graphene*
- [9] Yiwei Chen¹, Yan Huang¹, Qingxin Li¹, Bingbing Tong, Guangli Kuang, Chuanying Xi, Kenji Watanabe, Takashi Taniguchi, Guangtong Liu, Zheng Zhu, Li Lu, Fu-Chun Zhang, Ying-Hai Wu¹¹, and Lei Wang *Tunable even and odd-denominator fractional quantum Hall states in trilayer graphene*